

## Line tension between fluid phases and a substrate

T. Getta and S. Dietrich

*Fachbereich Physik, Bergische Universität Wuppertal, D-42097 Wuppertal, Germany*

(Received 13 June 1997)

We calculate the density distribution of a three-phase contact between the liquid-vapor interface of a simple fluid and a planar substrate. Using a microscopic density functional theory we pay particular attention to the long range of the underlying dispersion forces and find significant deviations from predictions of phenomenological theories. We monitor these structures and the corresponding line tension as a function of temperature upon approaching critical or first-order wetting transitions. [S1063-651X(97)02612-3]

PACS number(s): 68.45.Gd, 68.10.-m, 82.65.Dp

### I. INTRODUCTION

In thermal equilibrium the bulk of a thermodynamic phase is characterized by translational invariance—continuous for a fluid and discrete for a solid—of its local structural properties which give rise to the corresponding bulk free energy. Deviations from this translational invariance cause an excess in free energy which scales with the dimensionality of the defect. The most prominent example in the case of a three-dimensional bulk system is the surface tension  $\sigma_{\alpha\beta}$  which arises when, due to appropriate boundary conditions, two distinct phases  $\alpha$  and  $\beta$  of condensed matter in thermal equilibrium meet at a planar interface  $\alpha|\beta$  between them.

Under suitable thermodynamic conditions a system can exhibit three distinct phases  $\alpha$ ,  $\beta$ , and  $\gamma$  which are equally thermodynamically stable. Under these circumstances boundary conditions can be spatially arranged such that the system forms three interfaces  $\alpha|\beta$ ,  $\beta|\gamma$ , and  $\alpha|\gamma$  which meet at a line  $\alpha\beta\gamma$  [see Fig. 1(a)]. The excess free energy associated with this linear defect is called line tension  $\tau$  [1–3]. Figure 1(a) depicts the situation of an unconstrained thermal equilibrium as it can arise, e.g., in a binary liquid mixture where  $\alpha$  and  $\beta$  are two liquid phases rich in one and another species, respectively, and  $\gamma$  is the common vapor phase.

A line tension can, however, also occur in a constrained equilibrium where one of the phases, say the  $\alpha$  phase, is an inert spectator phase. To a large extent this is realized for a liquid-vapor interface  $\beta|\gamma$  exposed to a solid substrate  $\alpha$ . In this case the dihedral angle  $\theta_\alpha$  of the  $\alpha$  phase is prescribed geometrically; for a planar substrate it is  $\pi$  [see Fig. 1(b)]. In this case the dihedral angle of the  $\beta$  phase is called contact angle  $\theta$ . It characterizes the contact of a large volatile liquid drop with a solid substrate. Upon raising the temperature  $T$  the contact angle decreases and vanishes continuously at the wetting transition temperature  $T_w$  [4]. This implies that this system can support a distinct  $\alpha|\gamma$  interface only for  $T < T_w$  and the line tension is not defined for  $T > T_w$ .

In spite of its subdominance as compared with the surface tension, the line tension plays a significant role for a variety of important physical properties and phenomena such as the shape of small droplets [5,6], heterogeneous nucleation [7–10], dynamics of the contact line during spreading of drops [3,11], sticking and deformation of the contact line due to chemical heterogeneities of the substrate [12–14], the attachment of solid particles to a fluid interface [15], and formation

of Newton black films and foam films [16–20].

Nonetheless, as reviewed recently by Drelich [21], for most of the systems the magnitude and even the sign of the line tension are not known experimentally within an acceptable margin. Moreover, the spatial density distribution at the region of three-phase contact has not yet been resolved experimentally. Given this unsatisfactory experimental situation one is inclined to seek help from theoretical analyses. On the theoretical side the absence of translational invariance in *two* directions poses also a great challenge. Early theoretical work focused on the statistical description of the three-phase region, the contact angle, the line tension [22–26], various aspects of the line tension concerning the spreading of liquids on a substrate [27,28], local contact angles [29], the dependence of the contact angle on the droplet size [30,31], perturbations of the contact line [32,33], thin films [34–37], the detachment of sessile drops [38], and nucleation [39,40].

In the meantime the behavior of line tensions at wetting transitions has become an interesting subject in itself. The vanishing of the contact line at a wetting transition  $T_w$  leads to the question of a possibly singular behavior of the corresponding line tension. A vanishing line tension would be analogous to the vanishing surface tension of a liquid-vapor interface at the critical point. Early theoretical studies [41–43] gave conflicting answers to this question. Only recently has agreement with respect to certain aspects been achieved

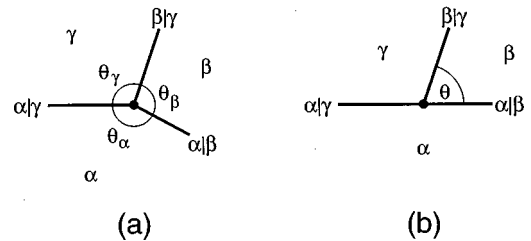


FIG. 1. Three bulk phases  $\alpha$ ,  $\beta$ , and  $\gamma$  in unconstrained (a) and constrained (b) thermodynamic equilibrium forming the interfaces  $\alpha|\beta$ ,  $\beta|\gamma$ , and  $\alpha|\gamma$  which meet at a triple line  $\alpha\beta\gamma$  whose cross section is denoted by a dot. The configuration is translationally invariant in the normal direction. In (a) the dihedral angles are determined by (see Ref. [2])  $\cos\theta_\alpha = (\sigma_{\beta\gamma}^2 - \sigma_{\alpha\beta}^2 - \sigma_{\alpha\gamma}^2) / (2\sigma_{\alpha\gamma}\sigma_{\beta\gamma})$ ,  $\cos\theta_\beta = (\sigma_{\alpha\gamma}^2 - \sigma_{\alpha\beta}^2 - \sigma_{\beta\gamma}^2) / (2\sigma_{\alpha\beta}\sigma_{\beta\gamma})$ , and  $\cos\theta_\gamma = (\sigma_{\alpha\beta}^2 - \sigma_{\alpha\gamma}^2 - \sigma_{\beta\gamma}^2) / (2\sigma_{\alpha\gamma}\sigma_{\beta\gamma})$ . In (b) the contact angle  $\theta$  is given by  $\cos\theta = (\sigma_{\alpha\gamma} - \sigma_{\alpha\beta}) / \sigma_{\beta\gamma}$ .

[44–56]. It has turned out that the type of singular behavior of the line tension upon approaching  $T_w$  depends on the range of the interactions and on the order of the wetting transition. At a first-order wetting transition the line tension does not vanish but either diverges or reaches a maximum value via a cusplike singularity. At a critical wetting transition the line tension vanishes at  $T_w$ . All those conclusions are based on mean-field theory. A good review of this subject is given by Indekeu [57]. Although already in 1981 Benner, Scriven, and Davis [58] had pointed out that in this context the description by local theories poses quantitative problems, all studies mentioned above are based on local gradient theories which neglect the nonlocal features induced by the long range of the dispersion forces acting in the fluid system. Recent studies of the line tensions associated with the formation of thin fluid films on geometrically [59] and chemically [60] structured substrates revealed very significant quantitative deficiencies of local gradient theories as compared with a fully nonlocal description. Encouraged by these results the purpose of the present study is to elucidate the relevance of long-ranged forces for the structure of the three-phase contact region and the corresponding line tension by comparing the predictions of the conventional local gradient theory with those obtained from a fully nonlocal description.

## II. STATISTICAL MECHANICS FOR THREE-PHASE CONTACT

### A. Boundary conditions

At first glance the most common realization of a three-phase contact line seems to be provided by a liquid drop in contact with its vapor and residing on a substrate. However, this system is only stable in the limiting case of a completely nonvolatile liquid in a canonical ensemble. Within equilibrium statistical mechanics this case is very difficult to implement. Instead the generic case to be considered by means of statistical mechanics is a fluid whose liquid and gas phase with number densities  $\rho_l$  and  $\rho_g$ , respectively, coexist in the bulk along a liquid-vapor coexistence curve  $\mu_0(T)$  of the chemical potential  $\mu$  which is constant throughout the sample. Near the substrate the requirement  $\mu = \text{const}$  induces spatial variations of the density in the direction normal to the substrate which we denote as the  $y$  direction. In the absence of a lateral corrugation of the substrate potential, which we assume to be the case in the following, the density profile  $\rho(y)$  does not depend on a lateral coordinate, say  $x$ . Consequently in such a grand canonical ensemble the drop configuration is unstable. The drop evaporates and one is left with a microscopically thin liquidlike film of thickness  $l_0(T)$  which can be inferred from the actual form of the equilibrium profile  $\rho(y)$ . Below the wetting transition temperature  $T_w$   $l_0(T)$  is finite whereas  $l_0$  becomes macroscopically large above  $T_w$ . This implies that for  $T < T_w$  and at coexistence  $\mu_0(T)$  one can maintain two distinct boundary conditions for the fluid at  $y \rightarrow \infty$ . The first one imposes that  $\rho(y \rightarrow \infty) = \rho_l$ . If the substrate prefers the liquid phase, a case which we consider in the following, this boundary condition leads to a sample completely filled with liquid up to substrate where the equilibrium substrate-liquid interface is formed and gives rise to the density profile  $\rho_+(y)$  for  $\mu \rightarrow \mu_0(T)$

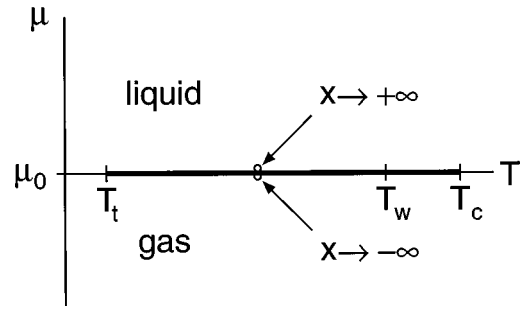


FIG. 2. Schematic phase diagram of liquid-gas coexistence at  $\mu_0$  between the triple temperature  $T_t$  and the critical temperature  $T_c$ . For simplicity  $\mu_0$  is taken to be temperature independent. Below the wetting transition temperature  $T_w$  the substrate remains nonwet if gas-liquid coexistence is approached from the gas side. If  $\mu_0$  is approached from the liquid side the whole sample is filled with liquid. If for  $x \rightarrow +\infty$  the latter boundary condition is applied and for  $x \rightarrow -\infty$  the former one, one obtains a density distribution as shown in Fig. 3.

+0. The second possible boundary condition imposes  $\rho(y \rightarrow \infty) = \rho_g$  leading to  $\rho_-(y)$  for  $\mu \rightarrow \mu_0(T) - 0$ .  $\rho_-(y)$  resembles the emerging substrate-liquid and the liquid-vapor interfaces separated by a distance  $l_0(T)$  of the liquidlike layer in between. At coexistence  $\mu = \mu_0(T)$  both profiles  $\rho_{\pm}(y)$  are equilibrium density distributions. This enables one to impose mixed boundary conditions in the lateral direction:  $\rho_-(y)$  for  $x \rightarrow -\infty$  and  $\rho_+(y)$  for  $x \rightarrow +\infty$  (see Fig. 2). This gives rise to a density distribution  $\rho(x, y)$  which interpolates smoothly between the limiting density distributions  $\rho_{\pm}(y)$  at  $x = \pm\infty$ . Defining the position of the liquid-vapor interface by, e.g.,  $\rho(x, y = l(x)) = \frac{1}{2}(\rho_l + \rho_g)$  renders a smooth interface profile  $l(x)$  which reduces to the value  $l_0(T)$  for  $x \rightarrow -\infty$  and which diverges for  $x \rightarrow +\infty$  (see Fig. 3). As the proper analysis of the various surface contributions to the

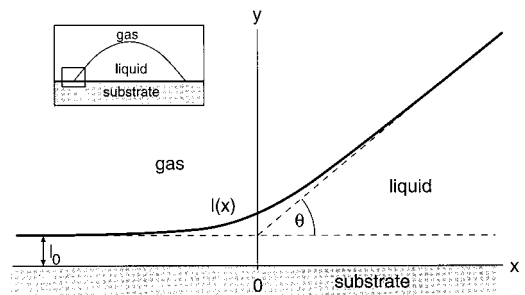


FIG. 3. Equilibrium density distribution resulting from the boundary conditions  $\rho(x = +\infty, y \rightarrow \infty) = \rho_l$  and  $\rho(x = -\infty, y \rightarrow \infty) = \rho_g$  at liquid-vapor coexistence  $\mu_0(T)$ .  $l(x)$  is the position of the suitably defined liquid-gas interface.  $l_0 = l(x \rightarrow -\infty)$  is the equilibrium thickness of the wetting film at  $T < T_w$  and at coexistence  $\mu_0(T)$ .  $l(x \rightarrow +\infty)$  diverges linearly such that the asymptote forms the contact angle  $\theta$  with the substrate. Under suitable conditions  $l(x)$  should resemble the density distribution of the three-phase contact region of a sessile liquid ridge. The actual shape of  $l(x)$  depends on the order of the wetting transition at  $T_w$ . The position  $x = 0$  is defined as the point at which the asymptotes of  $l(x)$  intersect. The density distribution is assumed to be translationally invariant in the  $z$  direction normal to the  $xy$  plane

free energy of this system shows, the above boundary conditions lead to a linear divergence of  $l(x \rightarrow +\infty)$  such that the asymptote of  $l(x \rightarrow +\infty)$  forms an angle  $\theta$  with the horizontal substrate which is the contact angle given by Young's law [see Fig. 1(b)]. In this sense the tacit hypothesis is that this well-defined equilibrium interface profile  $l(x)$  resembles the actual time-dependent density distribution at the three-phase contact line of a slowly evaporating, large, and volatile drop (see Fig. 3). Over which time scale this hypothesis is justified must be checked by an inherently dynamic theory.

### B. Density functional theory

Density functional theory has turned out to be successful for the description of spatially inhomogeneous fluids (see, e.g., Ref. [61]). Within this approach the equilibrium number density distribution minimizes the grand canonical free energy functional  $\Omega[\{\rho(\mathbf{r})\}; \mathbf{T}, \mu]$ :

$$\begin{aligned} \Omega[\{\rho(\mathbf{r})\}; T, \mu] = & \int_V d^3r f_{\text{HS}}(\rho(\mathbf{r}), T) \\ & + \frac{1}{2} \int_V d^3r \int_V d^3r' \tilde{w}(|\mathbf{r}-\mathbf{r}'|) \rho(\mathbf{r}) \rho(\mathbf{r}') \\ & + \int_V d^3r [\rho_w V(\mathbf{r}) - \mu] \rho(\mathbf{r}). \end{aligned} \quad (2.1)$$

$V$  is the finite volume occupied by the fluid in the half space  $V_+ = \{\mathbf{r} = (x, y, z) \in \mathbb{R}^3 | y \geq 0\}$ . In the thermodynamic limit, which will be considered carefully and in detail below, one has  $V \rightarrow V_+$ . For  $y < 0$  the fluid is contained by an inert wall with number density  $\rho_w$  exerting a substrate potential

$$V(y > 0) = - \sum_{i \geq 3} \frac{u_i}{y^i}. \quad (2.2)$$

In a simple approximation  $V(y)$  can be regarded to result from the pairwise summation of Lennard-Jones wall-fluid pair potentials

$$\phi_{wf}(r) = 4\epsilon_w [(\sigma_w/r)^{12} - (\sigma_w/r)^6]. \quad (2.3)$$

In this case the coefficients  $u_3 > 0$ ,  $u_4$ , and  $u_9 < 0$  are determined by  $\epsilon_w$ ,  $\sigma_w$ , and the lattice spacing of the substrate material. In the following, however, we consider  $u_3$ ,  $u_4$ , and  $u_9$  as the primary independent substrate potential parameters. The pair potential between the fluid particles is taken as

$$\phi(r) = 4\epsilon [(\sigma/r)^{12} - (\sigma/r)^6]. \quad (2.4)$$

Following the Barker-Henderson scheme [62]  $\phi(r)$  is split into an attractive part

$$\tilde{w}(r) = \begin{cases} \phi(r), & r \geq \sigma \\ 0, & r < \sigma \end{cases} \quad (2.5)$$

and into a repulsive part  $\phi(r \leq \sigma)$ . Whereas the former is treated perturbatively in Eq. (2.1) the latter part gives rise to a reference free energy density  $f_{\text{HS}}(\rho, T)$  of a hard sphere fluid with an effective hard sphere diameter

$$d(T) = \int_0^\sigma dr \{1 - \exp[-\phi(r)/(k_B T)]\}. \quad (2.6)$$

For the reference free energy we adopt the Carnahan-Starling approximation [63,64]:

$$f_{\text{HS}}(\rho, T) = k_B T \rho \left( \ln \eta - 1 + \frac{4\eta - 3\eta^2}{(1-\eta)^2} \right), \quad (2.7)$$

with

$$\eta = \frac{\pi}{6} \rho [d(T)]^3. \quad (2.8)$$

We emphasize that the functional used in Eq. (2.1) represents a simple version of density functional. It has the virtue of describing wetting transitions properly [4,65,66] although it does not capture fully the density oscillations which occur on an atomic scale  $\sigma$  close to the substrate due to packing effects. We are prepared to accept this latter deficiency because we shall focus on mesoscopic scales larger than  $\sigma$ . Finally we mention that in accordance with Eq. (2.1) we do not consider the effects of gravity.

For a bulk system with homogeneous density  $\rho(\mathbf{r}) = \rho_\gamma$ ,  $\gamma = l, g$ , Eq. (2.1) yields the bulk free energy density

$$\Omega_b(\rho_\gamma, T, \mu) = f_{\text{HS}}(\rho_\gamma, T) + \frac{1}{2} w_0 \rho_\gamma^2 - \mu \rho_\gamma, \quad (2.9)$$

where

$$w_0 = \int_{\mathbb{R}^3} d^3r \tilde{w}(r) = -\frac{32}{9} \pi \epsilon \sigma^3. \quad (2.10)$$

The requirements of two-phase coexistence between the equilibrium gas and liquid densities, i.e.,

$$\left. \frac{\partial \Omega_b}{\partial \rho} \right|_{\rho=\rho_g} = 0 = \left. \frac{\partial \Omega_b}{\partial \rho} \right|_{\rho=\rho_l}$$

and  $\Omega_b(\rho_g) = \Omega_b(\rho_l)$ , lead to the bulk phase diagram shown in Fig. 4.

### C. Surface free energy

In the case of a homogeneous boundary condition for  $y \rightarrow +\infty$  the density distribution will depend only on  $y$  so that the free energy functional decomposes into the bulk contribution given by Eq. (2.9) and into a surface contribution proportional to the area  $A$  of the substrate:

$$\Omega[\{\rho(y)\}; T, \mu] = V \Omega_b[\rho_\gamma; T, \mu] + A \Omega_s[\{\rho(y)\}; T, \mu]. \quad (2.11)$$

Accordingly this leads to the surface tensions

$$\sigma_{\alpha\beta}(T, \mu) = \min_{\rho(y)} \{ \Omega_s[\{\rho(y)\}; T, \mu] \}, \quad (2.12)$$

where  $(\alpha, \beta) = (w, l)$  corresponds to the boundary condition  $\rho(y \rightarrow \infty) = \rho_l$ ,  $(\alpha, \beta) = (w, g)$  to  $\rho(y \rightarrow \infty) = \rho_g$ , and  $(\alpha, \beta) = (l, g)$  to  $\rho(y \rightarrow \infty) = \rho_g$  and  $\rho(y \rightarrow -\infty) = \rho_l$  for  $V(y) \equiv 0$ .  $\sigma_{lg}(T)$  is only defined for  $\mu = \mu_0(T)$ ; in this case the

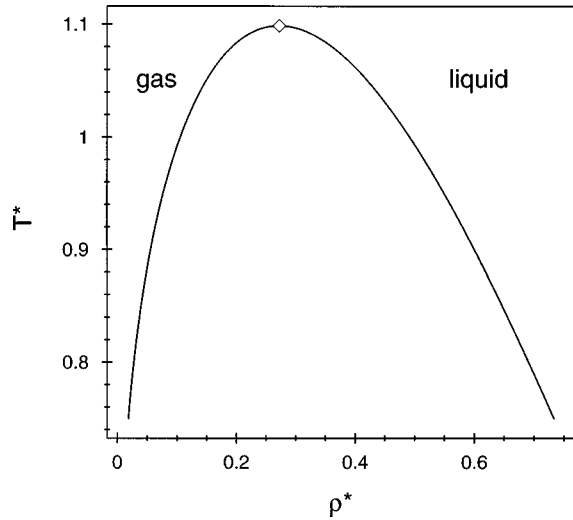


FIG. 4. Liquid-gas bulk phase diagram in terms of  $T^* = k_B T / \epsilon$  and  $\rho^* = \rho \sigma^3$  as predicted by Eqs. (2.1) and (2.4)–(2.8). The critical point ( $\diamond$ ) is given by  $(T_c^*, \rho_c^*) = (1.0986, 0.2722)$ . Freezing starts below the triple point  $T_i^* \lesssim 0.75$  which, however, is not captured by the simple density functional used in Eq. (2.1).

minima corresponding to  $\sigma_{wl}$  and  $\sigma_{wg}$  are given by  $\rho_+(y)$  and  $\rho_-(y)$ , respectively, as discussed in Sec. II A.

It has turned out [4] that wetting properties of such a system are described surprisingly well by applying the so-called sharp-kink approximation within which the minimization in Eq. (2.12) is restricted to the subspace of piecewise constant density profiles (see Fig. 5). Inserting a trial function as shown in Fig. 5 with a variable film thickness  $l$  into Eqs. (2.1) and (2.12) leads to the so-called effective interface potential [67,68]

$$\Omega_s(l; T, \mu) = l \Delta \Omega + \sigma_{wl} + \sigma_{lg} + \omega(l). \quad (2.13)$$

The linearly increasing term  $l \Delta \Omega$  with  $\Delta \Omega = \Omega_b(\rho_l, T, \mu_0) - \Omega_b(\rho_g, T, \mu) > 0$  corresponds to the price of building up a liquidlike film of thickness  $l$  in contact with an undersaturated vapor phase in the bulk. At two-phase coexistence one

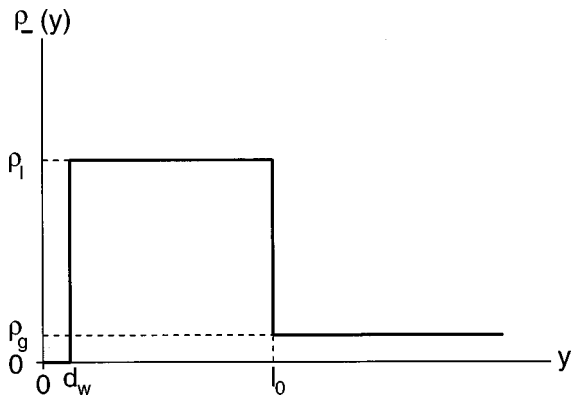


FIG. 5. Sharp-kink approximation of the number density profile  $\rho_-(y)$  corresponding to an equilibrium wetting film thickness  $l_0$ .  $d_w \approx (\sigma_w + \sigma) / 2$  describes the excluded volume due to the repulsive part of the substrate potential. The corresponding approximation for  $\rho_+(y)$  yields a profile which equals  $\rho_l$  for  $y > d_w$  and which is zero for  $y < d_w$ .  $\rho_l$  and  $\rho_g$  are taken at coexistence  $\mu_0(T)$  (see Fig. 4).

has  $\Delta \Omega = 0$ ;  $\sigma_{wl}$  denotes the wall-liquid surface tension (for the definition of  $d_w$  see Fig. 5)

$$\sigma_{wl} = -\frac{1}{2} \rho_l^2 \int_0^\infty dy t(y) - d_w \Omega_b(\rho_l) + \rho_l \rho_w \int_{d_w}^\infty dy V(y), \quad (2.14)$$

with

$$\begin{aligned} t(y) &= \int_y^\infty dy' \int_{-\infty}^\infty dx' \hat{w}(x'^2 + y'^2) \\ &= -\sum_{i \geq 3} \frac{t_i}{y^i}, \quad y \gg \sigma \end{aligned} \quad (2.15)$$

and

$$\hat{w}(x'^2 + y'^2) = \int_{-\infty}^\infty dz' \tilde{w}(\sqrt{x'^2 + y'^2 + z'^2}), \quad (2.16)$$

and  $\sigma_{lg}$  the liquid-gas surface tension

$$\sigma_{lg} = -\frac{1}{2} (\Delta \rho)^2 \int_0^\infty dy t(y), \quad (2.17)$$

where

$$\Delta \rho = \rho_l - \rho_g, \quad (2.18)$$

within the sharp-kink approximation. In Eq. (2.13)  $\omega(l)$  denotes the cost in free energy to maintain a wetting film of prescribed thickness  $l$  as compared to a configuration with  $l = \infty$ :

$$\begin{aligned} \omega(l) &= \Delta \rho \left( \rho_l \int_{l-d_w}^\infty dy t(y) - \rho_w \int_l^\infty dy V(y) \right) \\ &= \sum_{i \geq 2} \frac{a_i}{l^i}, \quad l \gg d_w. \end{aligned} \quad (2.19)$$

$a_2$  is known as the Hamaker constant. The equilibrium film thickness  $l_0(T, \mu)$  minimizes  $\Omega_s(l)$  and renders the wall-vapor surface tension:

$$\sigma_{wg} = \min_l \{ \Omega_s(l) \} = \Omega_s(l_0). \quad (2.20)$$

At coexistence, i.e.,  $\Delta \Omega = 0$ , this implies

$$\sigma_{wg} = \sigma_{lg} + \sigma_{wl} + \omega(l_0) \quad (2.21)$$

so that the contact angle is given by

$$\theta = \arccos \left( 1 + \frac{\omega(l_0)}{\sigma_{lg}} \right). \quad (2.22)$$

#### D. Shape of the liquid-gas interface

As discussed in Sec. II A mixed boundary conditions for  $y \rightarrow \infty$  lead to a laterally inhomogeneous density distribution  $\rho(x, y)$  with an interface profile  $l(x)$  as shown in Fig. 3. The asymptotic behavior of  $l(x)$  for large  $|x|$  is determined by the equilibrium *surface* contributions to the free energy:

$$l(x \rightarrow -\infty) = l_0 \quad (2.23)$$

and

$$l(x \rightarrow +\infty) = l_0 + x \tan \theta. \quad (2.24)$$

The lateral inhomogeneity of  $\rho(x, y)$  adds a line contribution  $L_z \Omega_l[\rho(x, y); T, \mu]$  to the free energy beyond the bulk and surface terms in Eq. (2.11). The line contribution scales with the linear extension  $L_z$  of the sample in that direction in

which it still displays translational invariance. By inserting the local sharp-kink approximation

$$\hat{\rho}(x, y) = \Theta(y - d_w) \{ \rho_l \Theta(l(x) - y) + \rho_g \Theta(y - l(x)) \} \quad (2.25)$$

into Eq. (2.1) a systematic analysis yields in the thermodynamic limit the following expression for the line contribution:

$$\begin{aligned} \lim_{L_z \rightarrow \infty} \frac{\Omega_l[\{l(x)\}; T, \mu]}{L_z} &= \int_{-\infty}^{\infty} dx [l(x) - d_w] \Delta f_{\text{HS}} + (\rho_g \rho_l - \rho_l^2) \int_{-\infty}^{\infty} dx \int_{-\infty}^{\infty} dx' \int_{l(x)}^{\infty} dy \int_{d_w}^{\infty} dy' \hat{w}[(x-x')^2 + (y-y')^2] \\ &+ \frac{1}{2} (\Delta \rho)^2 \int_{-\infty}^{\infty} dx \int_{-\infty}^{\infty} dx' \int_{l(x)}^{\infty} dy \int_{l(x')}^{\infty} dy' \hat{w}[(x-x')^2 + (y-y')^2] + \int_{-\infty}^{\infty} dx \int_{d_w}^{l(x)} dy \rho_w \Delta \rho V(y) \\ &- \int_{-\infty}^{\infty} dx [l(x) - d_w] \mu \Delta \rho, \end{aligned} \quad (2.26)$$

where

$$\Delta f_{\text{HS}} = f_{\text{HS}}(\rho_l) - f_{\text{HS}}(\rho_g). \quad (2.27)$$

The minimization of the line contribution with respect to  $l(x)$ , i.e.,  $\delta \Omega_l / \delta l(x) = 0$ , leads to the following nonlocal and nonlinear integral equation for the equilibrium interface profile  $\bar{l}(x)$ :

$$\begin{aligned} \Delta \Omega - \Delta \rho [\rho_l t(\bar{l}(x)) - \rho_w V(\bar{l}(x))] \\ = -(\Delta \rho)^2 \int_{-\infty}^{\infty} dx' \int_0^{\bar{l}(x') - \bar{l}(x)} dy' \hat{w}[(x-x')^2 + y'^2]. \end{aligned} \quad (2.28)$$

By enforcing a gradient expansion to the nonlocal expression on the right hand side of Eq. (2.28) one can approximate Eq. (2.28) by a local nonlinear differential equation [69]:

$$\begin{aligned} \Delta \Omega - \Delta \rho [\rho_l t(\bar{l}(x)) - \rho_w V(\bar{l}(x))] \\ = \sigma_{lg} \frac{d^2 \bar{l}(x)}{dx^2} \left[ 1 + \left( \frac{d\bar{l}(x)}{dx} \right)^2 \right]^{-3/2} + O((\bar{l}'')^2, \bar{l}'''). \end{aligned} \quad (2.29)$$

We note that the right hand side of Eq. (2.29) equals the negative functional derivative of  $\sigma_{lg} \int dx \sqrt{1 + [d\bar{l}(x)/dx]^2}$  which is the phenomenological expression for the cost in free energy due to the increased surface area of the configuration  $\bar{l}(x)$  as compared to the flat one  $\bar{l}(x) = \text{const}$ , disregarding curvature contributions. For a detailed assessment of the reliability of this phenomenological and local approximation see Refs. [69–72]. It turns out that for long-ranged forces decaying like a power law the coefficients of the higher-order terms on the right hand side of Eq. (2.29) become infinitely large so that the gradient expansion breaks down.

The consequences of this failure have been studied for the structure of the free liquid-vapor interface [69–72] and for the morphology of wetting films on geometrically [59] or chemically [60] structured substrates. Since in these cases the quantitative differences between the common phenomenological, but local, approach and the correct nonlocal expression have turned out to be very significant, in the following we want to compare the different predictions of the local [Eq. (2.29)] and the nonlocal [Eq. (2.28)] equation, respectively, for the shape of the interface at three-phase contact. As demonstrated by Fig. 7 in Ref. [60] for the case of a chemically inhomogeneous substrate the nonlocal theory is in close agreement with the full theory [Eq. (2.1)] in which one refrains from introducing an interface model and takes fully into account also the smooth density variation across the interface position. Therefore the nonlocal interface theory can be regarded as a reliable approximation.

### III. ANALYSIS OF THE SHAPE OF THE INTERFACE

The analysis of Eqs. (2.26) and (2.28) requires the numerical evaluation of multiple integrals of the potential function  $\hat{w}(x'^2 + y'^2)$  [see Eq. (2.16)] following from  $\tilde{w}(r)$ . For the actual nonanalytic form of  $\tilde{w}(r)$  [see Eq. (2.5)] these integrals cannot be carried out analytically which increases the numerical difficulties significantly. In order to avoid that we approximate  $\tilde{w}(r)$  by the following analytic form [73]:

$$\tilde{w}(r) = w_0 \frac{4\sigma^3}{\pi^2} (\sigma^2 + r^2)^{-3} \quad (3.1)$$

so that Eq. (2.10) remains valid with

$$\hat{w}(x^2 + y^2) = \frac{3w_0}{2\pi\sigma^2} (1 + \bar{x}^2 + \bar{y}^2)^{-5/2} \quad (3.2)$$

and

$$t(x) = \frac{w_0}{\pi} \left( \frac{\pi}{2} - \arctan(\bar{x}) - \frac{\bar{x}}{1+\bar{x}^2} \right), \quad (3.3)$$

where  $\bar{x} = x/\sigma$  and  $\bar{y} = y/\sigma$ . For this model one has [see Eq. (2.15)]

$$t_3 = -\frac{2}{3} \frac{w_0}{\pi} \sigma^3 = \frac{64}{27} \epsilon \sigma^6 > 0,$$

$t_4 = 0$ , and

$$t_5 = -\frac{6}{5} \frac{w_0}{\pi} \sigma^5 = \frac{192}{45} \epsilon \sigma^8 > 0.$$

The effective interface potential [Eq. (2.19)] is given by

$$\begin{aligned} \omega(l) = (\Delta\rho\sigma^3) & \left\{ -\frac{32}{9} \frac{\epsilon}{\sigma^2} (\rho_l\sigma^3) \right. \\ & \times \left[ 1 + [(l-d_w)/\sigma] \left( \arctan[(l-d_w)/\sigma] - \frac{\pi}{2} \right) \right] \\ & \left. + \rho_w\sigma^{-3} \sum_{i \geq 2} \frac{1}{i} \frac{u_{i+1}}{l^i} \right\} \end{aligned} \quad (3.4)$$

so that [see Eq. (2.19)]

$$a_2 = \frac{1}{2} \Delta\rho(\rho_w u_3 - \rho_l t_3), \quad (3.5)$$

$$a_3 = \frac{1}{3} \Delta\rho(\rho_w u_4 - 3\rho_l t_3 d_w), \quad (3.6)$$

and

$$a_4 = \frac{1}{6} \Delta\rho\rho_l(t_5 - 9t_3 d_w^2). \quad (3.7)$$

### A. Properties of the homogeneous wetting film

The thickness of the homogeneous wetting film corresponds to the position  $l_0$  of the minimum of the effective interface potential  $\omega(l)$  [Eq. (2.19)]. Figures 6 and 7 display a first-order and a critical wetting transition, respectively, together with the corresponding temperature dependence of the contact angle  $\theta$ . In both cases  $\theta$  vanishes continuously at the wetting transition temperature  $T_w$ . For first-order wetting one has  $\theta(\tau = (T_w - T)/T_w \rightarrow 0) \sim \tau^{1/2}$  and  $\theta(\tau \rightarrow 0) \sim \tau^{3/2}$  for critical wetting [4]. The potential parameters leading to Figs. 6 and 7 will be used in the following for calculating the inhomogeneous interface profile.

### B. Interface profile in local approximation

For the interaction potential parameters used for Figs. 6 and 7 we have solved the differential equation (2.29) at co-existence  $\Delta\Omega = 0$  with the boundary condition  $l(|x| \rightarrow \infty) = a(x)$  where

$$a(x) = l_0 \Theta(-x) + (l_0 + x \tan\theta) \Theta(x). \quad (3.8)$$

$\Theta(x)$  is the Heaviside function;  $a(x)$  has a break in slope at  $x=0$  which is defined as the position of the intersection between the asymptotes of  $l(x)$ . We found that the slope of the asymptote as obtained from the numerical solution  $l(x \gg \sigma)$  agrees with  $\tan\theta$  as obtained independently from Eq. (2.22)

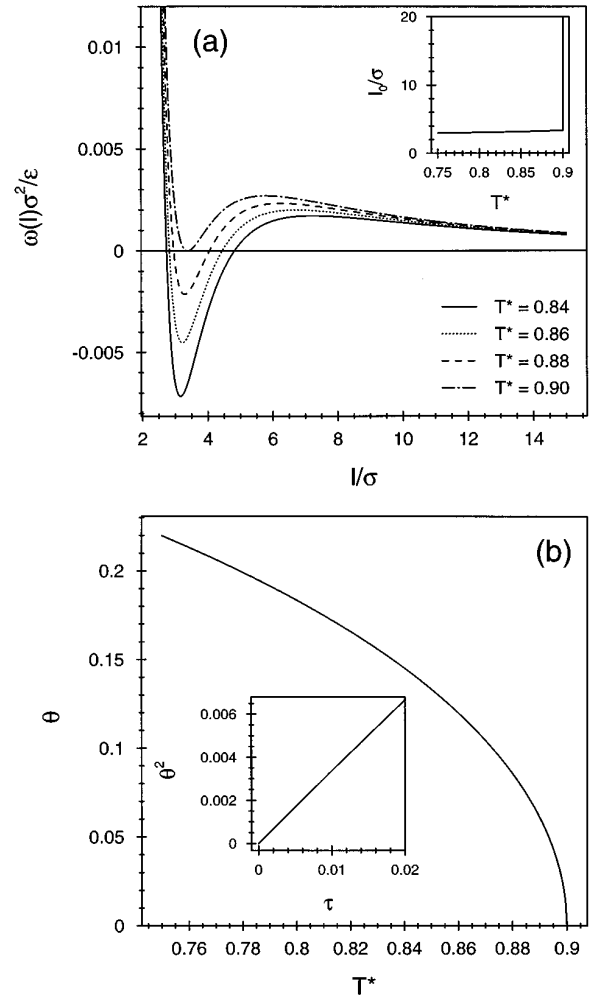


FIG. 6. (a) The effective interface potential  $\omega(l)$  [see Eq. (3.4)] for a first-order wetting transition for various temperatures  $T^* = k_B T/\epsilon$ . The equilibrium thickness  $l_0$  increases slightly as a function of  $T$  and jumps to infinity at the first-order wetting transition temperature  $T_w^* = 0.9$ . The contact angle  $\theta$  (in rad) vanishes  $\sim \tau^{1/2}$  for  $\tau = (T_w - T)/T_w \rightarrow 0$  (b). Here we have used the following interaction potential parameters:  $u_3 = 2.348\epsilon\sigma^6$ ,  $u_9 = -5.326\epsilon\sigma^{12}$ ,  $u_i = 0$  for  $i \neq 3, 9$ ,  $d_w = \sigma$ ,  $\rho_w = \sigma^{-3}$ . The potential parameters  $\epsilon$  and  $\sigma$  scale out by using reduced quantities.

to within  $10^{-6}$ . [Here and in the following we omit the overbar of  $l(x)$  indicating the equilibrium profile.] Figures 8 and 9 show the profile and the deviation

$$\delta l(x) = l(x) - a(x) \quad (3.9)$$

from the asymptotic behavior for first-order wetting and critical wetting, respectively. For a first-order wetting transition  $l(x \rightarrow \infty)$  approaches its asymptote from below so that  $\delta l(x > 0) < 0$  whereas  $l(x \rightarrow \infty)$  approaches its asymptote from above for critical wetting so that in this case  $\delta l(x > 0) > 0$ . In both cases  $l(x \rightarrow -\infty)$  approaches its asymptote  $l_0$  from above so that always  $\delta l(x < 0) > 0$ . For first-order wetting this positive part of  $\delta l(x < 0)$  is barely visible on the scales of Fig. 8. For critical wetting  $\delta l(x < 0)$  is substantially larger and comparable with  $\delta l(x > 0)$  although  $\delta l(x)$  vanishes more rapidly for  $x \rightarrow -\infty$  than for  $x \rightarrow \infty$ . We have found that, irrespective of the order of the transition,

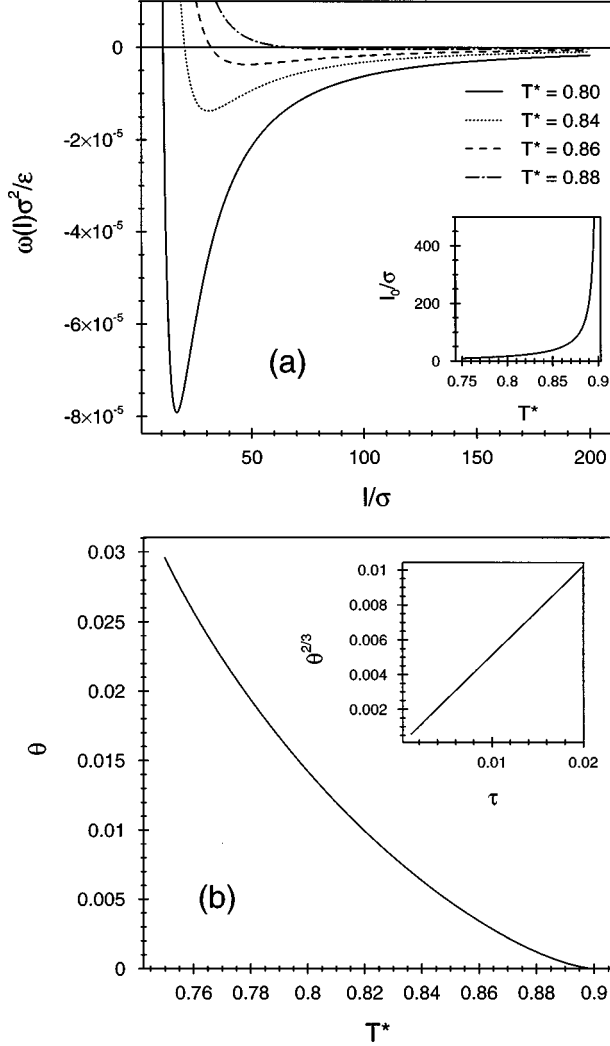


FIG. 7. (a) The effective interface potential  $\omega(l)$  [see Eq. (3.4)] for critical wetting for various temperatures  $T^*$ . The equilibrium thickness  $l_0$  diverges  $\sim \tau^{-1}$  for  $\tau = (T_w - T)/T_w \rightarrow 0$ ; here  $T_w^* = 0.9$ . The contact angle  $\theta$  (in rad) vanishes  $\sim \tau^{3/2}$  (b). Here we have used the following interaction potential parameters:  $u_3 = 1.423\epsilon\sigma^6$ ,  $u_4 = 9.000\epsilon\sigma^6$ ,  $u_g = -0.190\epsilon\sigma^{12}$ ,  $u_i = 0$  for  $i \neq 3, 4, 9$ ,  $d_w = \sigma$ ,  $\rho_w = \sigma^{-3}$ .

$\delta l(x \rightarrow -\infty) \sim |x|^{-3}$  and  $\delta l(x \rightarrow \infty) \sim x^{-2}$ . There is a huge difference of the magnitude and of the extent of the deviation of the profile from its asymptotes between first-order and critical wetting. At comparable temperatures the deviation is about an order of magnitude larger and two orders of magnitude wider for critical wetting than for first-order wetting. Irrespective of the order of the transition the deviation  $\delta l(x)$  increases upon approaching  $T_w$  and reaches a mesoscopic scale.

By using a phenomenological local interface displacement model Indekeu [46] has obtained qualitatively similar results. In the present context the above findings, which are based on a microscopic model instead of on a phenomenological ansatz, are needed to serve for a quantitative comparison in order to test the reliability of the local theory versus the actual nonlocal one.

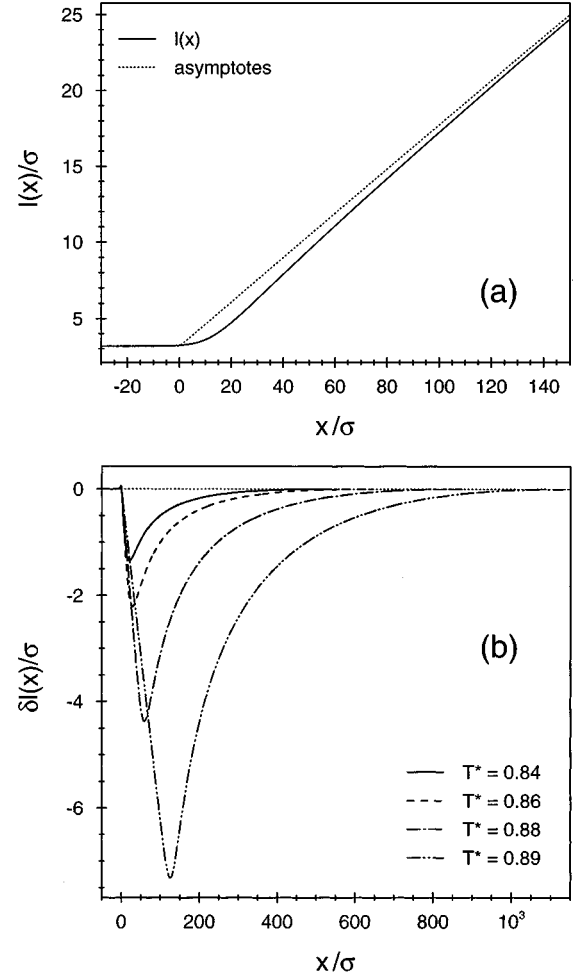


FIG. 8. (a) Shape of the profile  $l(x)$  of the liquid-gas interface at  $T^* = 0.84$  for a first-order wetting transition within local approximation using the interaction potential parameters as in Fig. 6. The wetting temperature is  $T_w^* = 0.9$ . The dotted line is the asymptote  $a(x)$ . The angle given by the slope of the asymptote gives the contact angle  $\theta$  at  $T^* = 0.84$ . (b) Deviation  $\delta l(x) = l(x) - a(x)$  of the profile from its asymptotes for various temperatures.

### C. Interface profile from nonlocal theory

We have solved the nonlocal integral equation (2.28) for  $\Delta\Omega = 0$  by applying a suitable iteration scheme to its discretized version. It is a significant challenge to find the correct solution and requires a substantial numerical effort. Based on the same interaction potential parameters as for the local approach Figs. 10 and 11 show the corresponding results for  $\delta l(x)$  within the nonlocal theory for first-order wetting and critical wetting, respectively, as well as a direct comparison between the predictions of the local and the nonlocal theory. These theories agree insofar as they both predict that in the case of first-order wetting the profile  $l(x \rightarrow \infty)$  approaches its asymptote from below whereas it approaches its asymptote from above for critical wetting. However, as Figs. 10 and 11 demonstrate, the quantitative differences are very large and increase upon approaching  $T_w$ . Generally speaking the local theory overestimates significantly both the extent and the width of the deviation of the profile from its asymptotes. In the case of first-order wetting the maximum

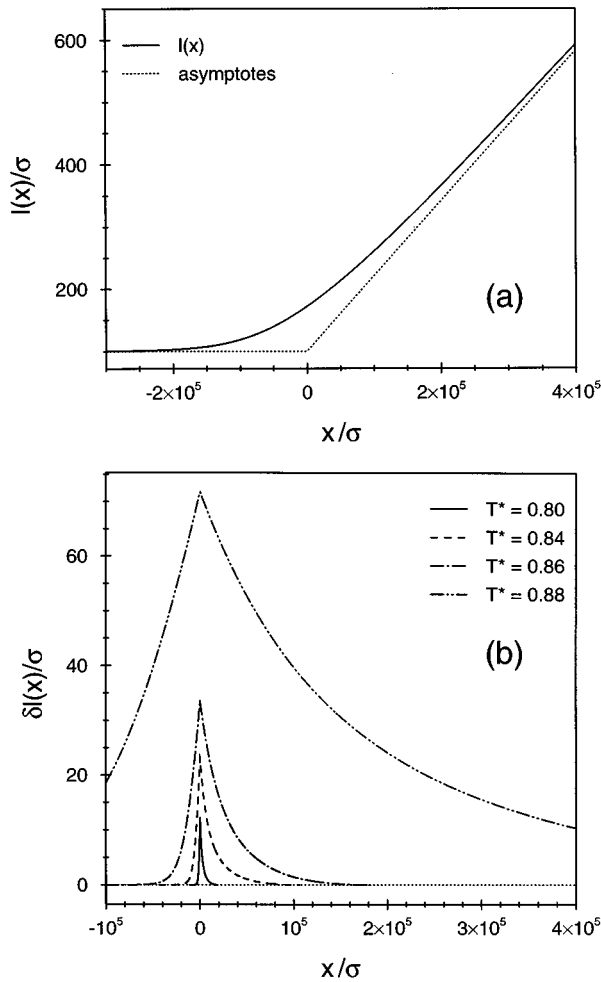


FIG. 9. (a) Shape of the profile  $l(x)$  of the liquid-gas interface at  $T^* = 0.88$  for the critical wetting transition shown in Fig. 7 within local approximation. The wetting temperature is  $T_w^* = 0.9$ . The dotted line is the asymptote  $a(x)$ . The angle given by the slope of the asymptote gives the contact angle  $\theta$  at  $T^* = 0.88$ . (b) Deviation  $\delta l(x) = l(x) - a(x)$  of the profile from its asymptotes for various temperatures.

deviation and the width of  $\delta l(x)$  are predicted by a factor of 4 too large by the local theory; according to the nonlocal theory the maximum deviations occur much closer to  $x=0$  than predicted by the local theory. For first-order wetting the deviation  $\delta l(x)$  has a sizable value only for  $x > 0$ . However, for critical wetting  $\delta l(x)$  is more equally distributed around  $x=0$ . Even at a low temperature the width of  $\delta l(x)$  for critical wetting is more than ten times larger than for first-order wetting. Since this width increases further with temperature the corresponding numerical difficulties limited our evaluation of the nonlocal theory in the case of critical wetting to low temperatures. For critical wetting the discrepancies between local and nonlocal theory are even more pronounced. The local theory overestimates the maximum deviation and the width by a factor of 20 and 5, respectively.

A surprising result of the nonlocal theory is that the absolute value of the deviation of  $l(x)$  from its asymptotes is at most on the order of a molecular diameter. However, the width of this small deviation is several hundred molecular diameters. Thus a major finding of the nonlocal analysis is

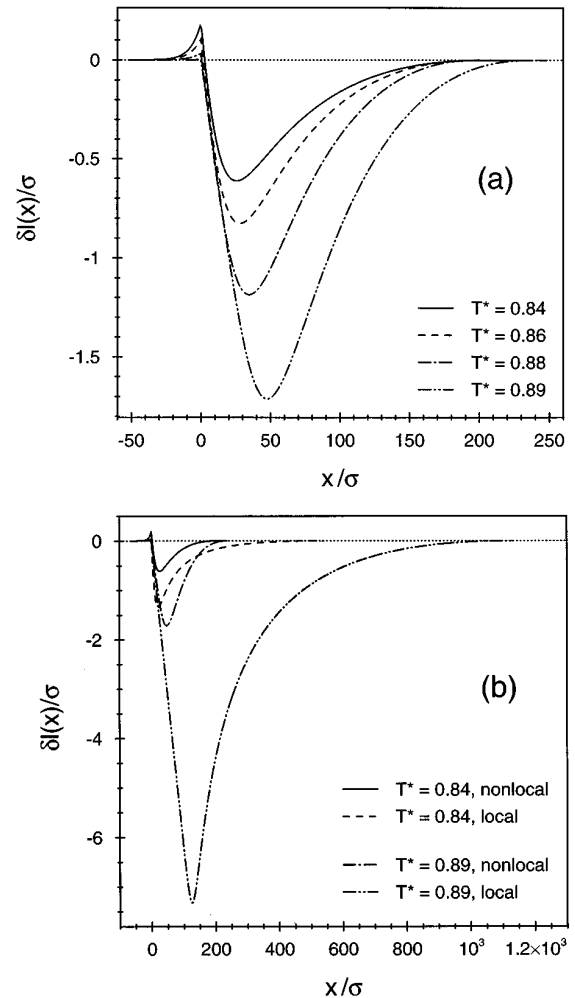


FIG. 10. (a) Deviation of the interface profile from its asymptotes as obtained from the nonlocal theory upon approaching a first-order wetting transition at  $T_w^* = 0.9$ . The interaction potential parameters are the same as for Fig. 6. (b) Direct comparison between the predictions of the local and the nonlocal theory for two temperatures.

that the interface profile follows its asymptotes rather closely.

Figure 12 provides a close look at the temperature dependence of the width  $\Delta x$  of  $\delta l(x)$ . To be specific we define  $\Delta x$  as that region within which  $|\delta l(x)/\sigma| > 10^{-3}$ . Figure 12 shows that for first-order wetting the local theory predicts a divergence of  $\Delta x$  for  $T \rightarrow T_w$  whereas within the nonlocal theory  $\Delta x$  seems to remain finite upon approaching  $T_w$  or to diverge only very close to  $T_w$ . Our numerical analysis indicates that irrespective of the order of the transition the local theory predicts a divergence  $\Delta x \sim \theta^{-3/2}$  for  $\theta \rightarrow 0$ . The comparison between Figs. 8(b) and 10(a) shows that the maximum deviation  $|\delta l_{\max}|$  clearly diverges within local theory whereas in the nonlocal theory it is much smaller, increases also, but a divergence is not yet visible.

It is interesting to note that for first-order wetting the local theory overestimates the curvature

$$K(x) = \frac{l''(x)}{[1 + l'(x)^2]^{3/2}} \quad (3.10)$$

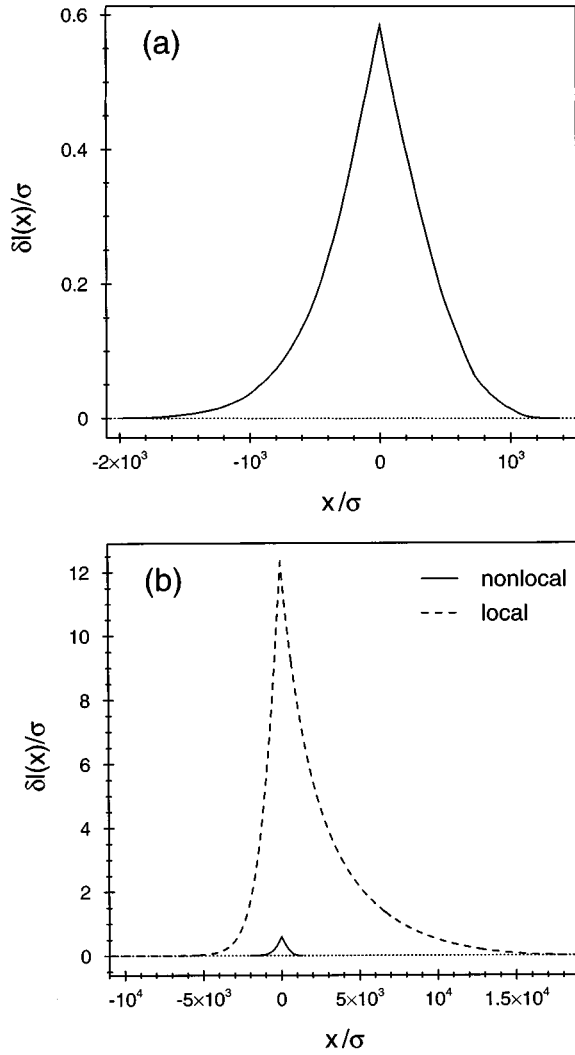


FIG. 11. (a) Deviation of the interface profile from its asymptotes as obtained from the nonlocal theory for  $T^* = 0.75$  in the case of a critical wetting transition at  $T_w^* = 0.9$ . (b) Direct comparison between the predictions of the local and the nonlocal theory for  $T^* = 0.75$ .

of the profile whereas it underestimates it significantly in the case of critical wetting (see Fig. 13). For critical wetting the curvature of  $l(x)$  is much smaller.

In the local theory the spatial inhomogeneity of the interface is penalized by a term  $\sigma_{lg} \int dx \sqrt{1 + [l'(x)]^2}$  [see Eq. (2.29)]. One could surmise that by treating  $\sigma_{lg}$  as a phenomenological parameter a suitable choice for  $\sigma_{lg}$  would allow one to map the profiles as obtained by the local theory onto those as obtained by the nonlocal theory. If this would be possible the deficiencies of the local theory would appear to be less dramatic. To this end we have varied the value for  $\sigma_{lg}$  entering the local theory by nearly three orders of magnitude. Figure 14 demonstrates that none of these profiles obtained from such an effective local theory is close to the profile predicted by the nonlocal theory. Therefore we conclude that in spite of its popularity the local theory is inadequate to describe the shape of the interface.

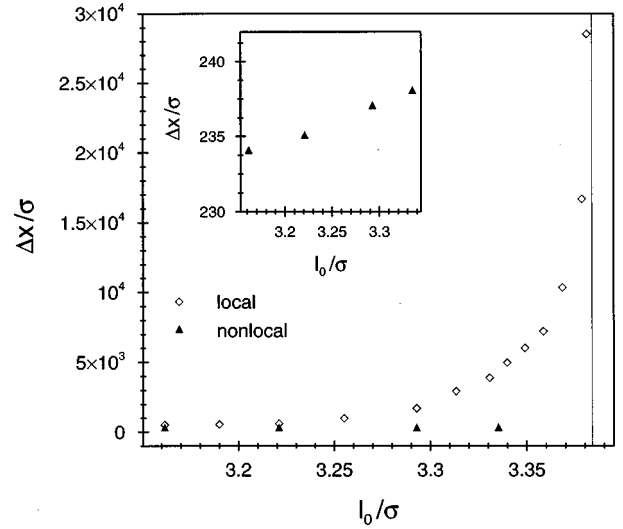


FIG. 12. The width  $\Delta x$  of the shape of the interface as a function of the layer thickness  $l_0$  for a first-order wetting transition, which occurs at  $l_0/\sigma = 3.3838$ , as obtained by the local and the nonlocal theory. The inset shows the data of the nonlocal theory on a smaller scale. The local theory predicts a divergence of  $\Delta x$  for  $T \rightarrow T_w$  whereas  $\Delta x$  increases only slightly in the nonlocal theory. Within the width  $\Delta x$  the deviation of the profile from its asymptotes is larger than  $10^{-3}\sigma$ .

#### IV. LINE TENSION

The explicit separation of the grand canonical free energy functional  $\Omega[\rho(\mathbf{r})]$  [Eq. (2.1)] into bulk, surface, and line contributions as well as the identification of all artificial terms generated by the finite sample volume  $V_f$  are carried out systematically in the Appendix. Within the sharp-kink approximation [Eq. (2.25)] the line contribution from the three-phase contact region consists of three distinct terms:

$$\tau[l(x)] = \tau_a[a(x)] + \tau_\omega[l(x)] + \tau_i[l(x)]. \quad (4.1)$$

The first term is solely determined by the asymptotes of the profile, i.e., by  $\theta$  and  $l_0$ :

$$\tau_a[a(x)] = \tilde{\tau}(\theta) + \bar{\omega}(l_0, \theta). \quad (4.2)$$

It is the sum of a contribution  $\tilde{\tau}(\theta)$  which depends on the interface profile only via the contact angle  $\theta$ ,

$$\begin{aligned} \tilde{\tau}(\theta) = & \frac{1}{2} (\Delta\rho)^2 \left[ 1 - \frac{\theta}{\tan\theta} \right] \\ & \times \int_0^\infty dx \int_0^\infty dy \int_{-\infty}^\infty dz \, xy \bar{w}(\sqrt{x^2 + y^2 + z^2}), \end{aligned} \quad (4.3)$$

and of a contribution  $\bar{\omega}(l_0, \theta)$  which is given explicitly in terms of the wetting film thickness  $l_0$  and  $\theta$  whose temperature dependences are given in Sec. II C [compare Eqs. (2.15) and (2.2)]:

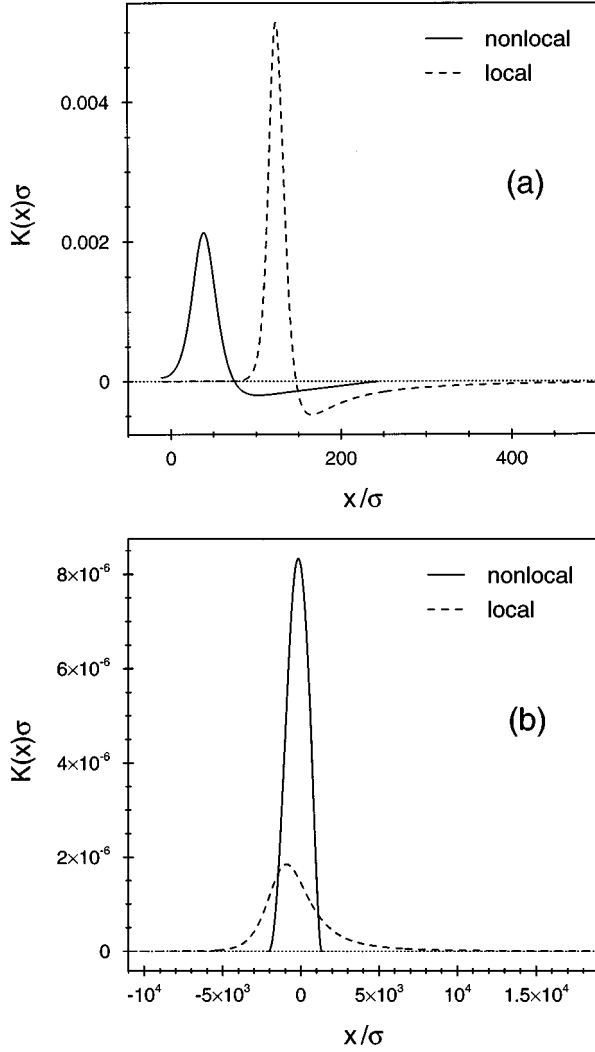


FIG. 13. Curvature of the interface profile as obtained by the local and nonlocal theory at  $T^*=0.89$  in the case of first-order wetting (a) and at  $T^*=0.75$  in the case of critical wetting (b).

$$\begin{aligned} \bar{\omega}(l_0, \theta) &= \frac{\Delta\rho}{\tan\theta} \int_0^\infty dy y \{ \rho_l t(y+l_0-d_w) - \rho_w V(y+l_0) \} \\ &= \frac{1}{\tan\theta} \int_{l_0}^\infty dl \omega(l) = \frac{1}{\tan\theta} \sum_{i \geq 1} \frac{1}{i} \frac{a_{i+1}}{l_0^i}. \end{aligned} \quad (4.4)$$

For the model discussed in Sec. III one has

$$\bar{\tau}(\theta) = -\frac{8}{9} \frac{\epsilon}{\sigma} (\Delta\rho\sigma^3)^2 \left( 1 - \frac{\theta}{\tan\theta} \right) < 0 \quad (4.5)$$

and

$$\begin{aligned} \bar{\omega}(l_0, \theta) &= \frac{\Delta\rho\sigma^3}{\tan\theta} \left( \frac{16}{9} \frac{\epsilon}{\sigma} (\rho_l\sigma^3) \left\{ \left[ \left( \frac{l_0-d_w}{\sigma} \right)^2 + 1 \right] \right. \right. \\ &\quad \times \left. \left. \left( -\frac{\pi}{2} + \arctan \frac{l_0-d_w}{\sigma} \right) + \frac{l_0-d_w}{\sigma} \right\} \right. \\ &\quad \left. + \rho_w\sigma^{-3} \sum_{i \geq 1} \frac{1}{i(i+1)} \frac{u_{i+2}}{l_0^i} \right). \end{aligned} \quad (4.6)$$

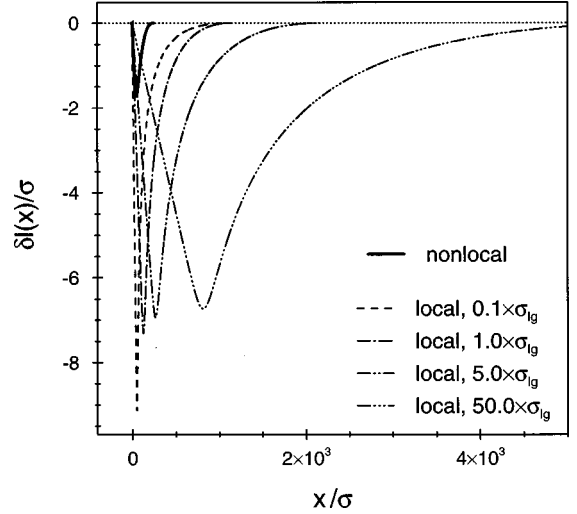


FIG. 14. Comparison of the deviation of the interface profile from its asymptotes as obtained by the nonlocal theory and by the local theory in which the surface tension  $\sigma_{lg}$  is changed between a factor of  $\frac{1}{10}$  and 50 of its actual value [Eq. (2.17)]. None of these local results resembles the nonlocal one. These calculations correspond to the case of first-order wetting and  $T^*=0.89$ .

In Eq. (4.1) the second term  $\tau_\omega[l(x)]$  does depend on the full interface profile and resembles an integrated local effective interface potential:

$$\begin{aligned} \tau_\omega[l(x)] &= -\Delta\rho \int_{-\infty}^\infty dx \int_{a(x)}^{l(x)} dy \{ \rho_l t(y-d_w) - \rho_w V(y) \} \\ &= \int_{-\infty}^\infty dx \{ \omega(l=l(x)) - \omega(l=a(x)) \}. \end{aligned} \quad (4.7)$$

One has  $\tau_\omega[l(x)=a(x)]=0$ . Whereas in Eq. (4.1) the second term  $\tau_\omega$  depends on both the fluid-fluid interaction potential and on the substrate potential the third term  $\tau_i$ , which also vanishes for  $l(x)=a(x)$ , is determined by the interaction between the fluid particles alone. Only this third term carries the difference between the nonlocal and the local theory. In the nonlocal theory one has

$$\begin{aligned} \tau_i^{(\text{nlloc})}[l(x)] &= \frac{1}{2} (\Delta\rho)^2 \int_{-\infty}^\infty dx \int_{a(x)}^{l(x)} dy \int_{-\infty}^\infty dx' \\ &\quad \times \left\{ \int_{-\infty}^{a(x')} dy' \hat{w}[(x-x')^2 + (y-y')^2] \right. \\ &\quad \left. - \int_{l(x')}^\infty dy' \hat{w}[(x-x')^2 + (y-y')^2] \right\}. \end{aligned} \quad (4.8)$$

The local approximation of  $\tau_i^{(\text{nlloc})}$  is given by

$$\begin{aligned} \tau_i^{(\text{loc})}[l(x)] &= \sigma_{lg} \int_{-\infty}^\infty dx \left\{ \left[ 1 + \left( \frac{dl(x)}{dx} \right)^2 \right]^{1/2} \right. \\ &\quad \left. - \left[ 1 + \left( \frac{da(x)}{dx} \right)^2 \right]^{1/2} \right\}, \end{aligned} \quad (4.9)$$

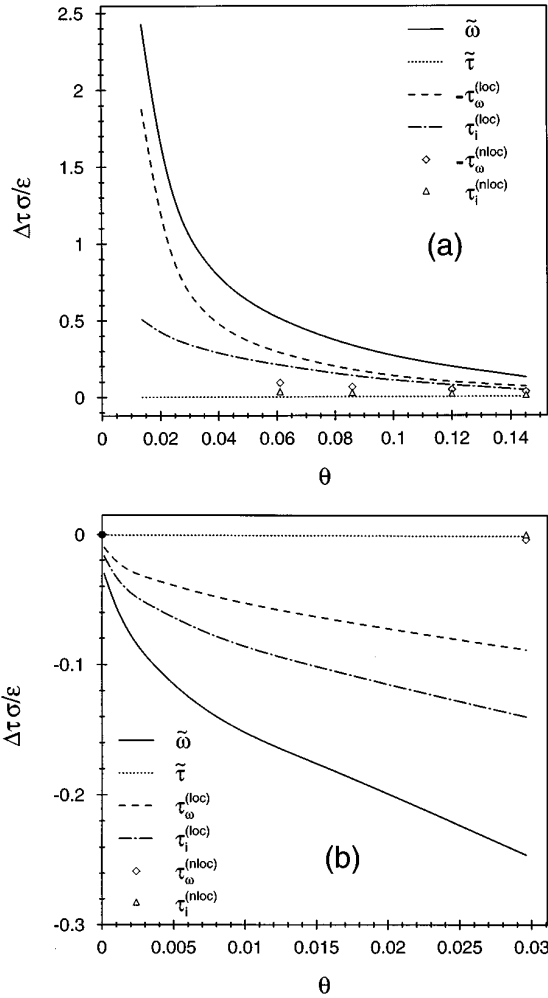


FIG. 15. Contact angle dependence (in rad) of the various contributions  $\Delta\tau = \bar{\omega}$ ,  $\bar{\tau}$ ,  $\tau_\omega$ , and  $\tau_i$  to the total line tension  $\tau$  within local and nonlocal theory for first-order wetting (a) and critical wetting (b) [see Eqs. (4.1)–(4.9)]. Note that in (a) we have plotted the absolute values of  $\tau_\omega^{(loc)}$  and  $\tau_\omega^{(nlc)}$ . In (a)  $\bar{\omega}$  diverges  $\sim 1/\theta$  for  $\theta \rightarrow 0$ .  $\tau_\omega^{(loc)}$  diverges as  $-\text{const}/\theta + \text{const} \times \ln(1/\theta)$  with both constants positive so that the leading singularities of  $\bar{\omega}$  and  $\tau_\omega^{(loc)}$  cancel. This implies that  $\bar{\omega} + \tau_\omega^{(loc)}$  diverges as  $\ln(1/\theta)$ . However, the gap between  $\bar{\omega}$  and  $-\tau_\omega^{(nlc)}$  seems to become much larger for  $\theta \rightarrow 0$  compared with the gap between  $\bar{\omega}$  and  $-\tau_\omega^{(loc)}$ . Therefore  $\bar{\omega} + \tau_\omega^{(nlc)}$  and thus  $\tau$  behave  $\sim 1/\theta$  over a wide range of contact angle values. However, in principle we cannot rule out that for very small values of  $\theta$  also  $\tau_\omega^{(nlc)}$  develops a singularity  $-\text{const}/\theta + \text{const} \times \ln(1/\theta)$  so that  $\bar{\omega} + \tau_\omega^{(nlc)}$  and thus  $\tau$  behave  $\sim \ln(1/\theta)$  as predicted by the local theory. But certainly this behavior would be confined to very small values of  $\theta$ . In (b)  $\bar{\omega}$ ,  $\tau_\omega^{(loc)}$ , and  $\tau_i^{(loc)}$  vanish  $\sim \theta^{1/3}$  for  $\theta \rightarrow 0$  (see the dot). Since  $|\tau_\omega^{(nlc)}|$  and  $|\tau_i^{(nlc)}|$  are negligibly small compared with the corresponding local expressions,  $\bar{\omega}$  is the dominant contribution. The situation is similar in (a). Thus irrespective of the order of the transition the total line tension is dominated by the contribution  $\bar{\omega}$ . The contribution  $|\bar{\tau}| \sim \theta^2$  is negligibly small in (a) and (b).

with  $\sigma_{lg}$  from Eq. (2.17) and  $da(x)/dx = \Theta(x)\tan\theta$ . The functional derivative  $\delta\tau[l(x)]/\delta l(x) = 0$  yields Eqs. (2.28) and (2.29) with  $\Delta\Omega_b = 0$  for the nonlocal and local theory, respectively.

It is instructive to compare in Fig. 15 the magnitude of

each contribution to the total line tension [Eq. (4.1)]. For the model we used the term  $\bar{\tau}(\theta) \approx \theta^2$  is always negligibly small. The dominant contribution is  $\bar{\omega}(l_0, \theta)$ . Upon approaching  $T_w$  it is approximately equal to  $a_2/\theta l_0$ . Since for first-order wetting  $a_2 > 0$  and  $l_0 < \infty$ ,  $\bar{\omega}(l_0, \theta)$  diverges  $\sim 1/\theta$  for  $\tau = (T_w - T)/T_w \rightarrow 0$  for first-order wetting. In case of critical wetting  $a_2 \sim -\tau \rightarrow 0^-$  and  $l_0 \sim 1/\tau$  so that with  $\theta \sim \tau^{3/2}$  one finds that  $\bar{\omega}(l_0, \theta)$  vanishes  $\sim \theta^{1/3}$ . Whereas this behavior of  $\bar{\omega}(l_0, \theta)$  is independent of using a local or a nonlocal interface theory, the remaining contributions  $\tau_\omega$  and  $\tau_i$  do depend on the kind of approach used. Within the local theory and for first-order wetting it turns out that  $\tau_\omega^{(loc)}$  behaves like  $-\text{const}/\theta + \text{const} \times \ln(1/\theta)$  with both constants positive such that the  $1/\theta$  singularity cancels the corresponding singularity of  $\bar{\omega}$  so that  $\bar{\omega} + \tau_\omega^{(loc)}$  diverges  $\sim \ln(1/\theta)$ . Since  $\tau_i^{(loc)}$  also diverges  $\sim \ln(1/\theta)$  in the case of the first-order wetting, one finds this kind of singularity for  $\tau$  itself. In the case of critical wetting all three contributions  $\bar{\omega}$ ,  $\tau_\omega^{(loc)}$ , and  $\tau_i^{(loc)}$  vanish  $\sim \theta^{1/3}$  without a compensation effect. This is in accordance with Indekeu's results [57] obtained from a local interface displacement model for the long-ranged forces considered here.

Within the nonlocal theory Fig. 15(b) demonstrates that in the case of critical wetting the term  $\bar{\omega}$  dominates completely all other contributions so that its singularity  $\sim \theta^{1/3}$  remains valid for the total line tension  $\tau$ , it also shows that within the nonlocal theory  $\tau$  is less negative than within the local theory. Whether the logarithmic singularity of  $\tau$  in case of first-order wetting remains valid also for the total line tension  $\tau$  within the nonlocal theory is less obvious. As described above, the occurrence of the logarithmic singularity relies on the cancellation of the  $1/\theta$  singularity of  $\bar{\omega}$  by a corresponding one in  $\tau_\omega^{(nlc)}$ . On the basis of the available data in Fig. 15(a) it is difficult to imagine that this compensation effect prevails also within the nonlocal theory. If not, one would find that  $\tau \sim 1/\theta$  instead of  $\ln(1/\theta)$ . Regrettably, due to numerical difficulties, we were unable to obtain data within the nonlocal theory for smaller values of  $\theta$ . This prevents us from ruling out the aforementioned cancellation mechanism so that we cannot exclude the possibility that also within the nonlocal theory  $\tau$  diverges  $\sim \ln(1/\theta)$ . But even if ultimately for  $\theta \rightarrow 0$  a logarithmic singularity would appear, Fig. 15(a) demonstrates that over a wide range of contact angles  $\tau$  appears to diverge  $\sim 1/\theta$  in case of first-order wetting. Since  $|\tau_\omega^{(nlc)}| < |\tau_\omega^{(loc)}|$  the line tension  $\tau$  within the nonlocal theory is larger as obtained within the local theory.

Figure 16 shows the numerical results for  $\tau$  in local and nonlocal approximation which were obtained by inserting the numerical solutions for the corresponding equilibrium profiles into Eqs. (4.1)–(4.9). For first-order wetting the local theory underestimates the line tension by about 20–80%. For critical wetting  $\tau$  is negative and vanishes within the local approximation for  $T \rightarrow T_w$  as  $\theta^{1/3}$  in agreement with the singularity found by Indekeu [46]. As described above we expect that this singularity also holds within the nonlocal theory. It turns out that for critical wetting the local theory overestimates  $|\tau|$  by about 25%. Away from  $T_w$  and irrespective of the order of the wetting transition the absolute value of the line tension is of the order of  $\epsilon/\sigma$ . This yields values

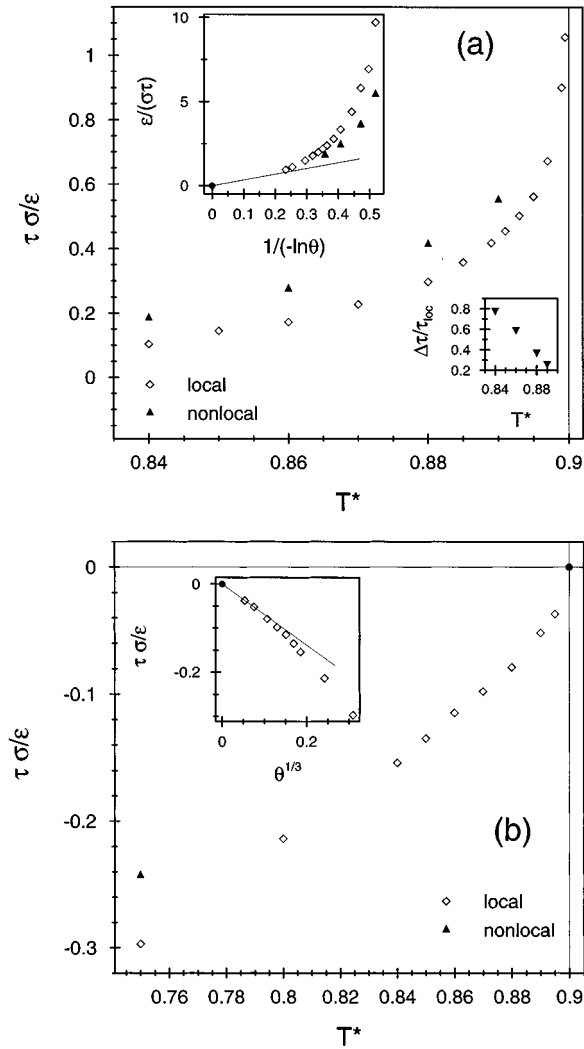


FIG. 16. Comparison of the prediction of the local and nonlocal theory for the line tension  $\tau$  for first-order wetting (a) and critical wetting (b). The data correspond to the systems studied in Figs. 6 and 7. In (a) the insets probe the logarithmic divergence  $\tau \sim -\ln\theta$  for  $T \rightarrow T_w$  and show the relative deviation  $\Delta\tau/\tau_{loc} = (\tau_{nl} - \tau_{loc})/\tau_{loc}$ , respectively. For critical wetting the local theory predicts that  $\tau$  vanishes  $\sim \theta^{1/3}$  for  $T \rightarrow T_w$  (see the inset).  $\theta$  is measured in rad. In both cases  $T_w^* = 0.9$ . For first-order wetting  $\tau$  is positive and for critical wetting  $\tau$  is negative. Away from  $T_w$   $\tau$  is of the order of  $\epsilon/\sigma$ .

of about  $10^{-11}$  J/m compared with experimental values ranging between  $10^{-5}$  and  $3 \times 10^{-12}$  J/m [21].

In Sec. III C we have found that the profile  $l(x)$  deviates only slightly from the asymptotes  $a(x)$ . Therefore one would surmise that  $\tau_a[a(x)]$  [see Eq. (4.2)] provides already a good approximation for the actual line tension  $\tau[l(x)]$  [Eq. (4.1)] which takes the smooth variation of  $l(x)$  fully into account. The inspection of Fig. 15 confirms this expectation. In the case of first-order wetting and sufficiently below  $T_w$  one finds that  $\tau_\omega$  is about 25% of  $\tau_a$  and  $\tau_i$  is about 5% of  $\tau_a$ ; furthermore  $|\tilde{\tau}|$  is much smaller than  $\tilde{\omega}$  [Eq. (4.2)]. Upon approaching  $T_w$  the contribution of  $\tilde{\omega}$  becomes even much more dominant than all the others. In the case of critical wetting for all temperatures the contributions  $\tilde{\tau}$ ,  $\tau_\omega$ , and  $\tau_i$  are negligibly small compared with  $\tilde{\omega}$ . These statements re-

fer to the results obtained from the nonlocal theory. Consistently we find that within the local theory, which predicts large deviations of  $l(x)$  from the asymptotes  $a(x)$ , the contributions  $\tau_i^{(loc)}$  and  $\tau_\omega[l_{loc}(x)]$  are smaller but comparable with the contribution  $\tilde{\omega}$ , which is independent from the type of theory used. Therefore we conclude that Eqs. (4.4) and (4.6) provide a rather accurate estimate for the actual value of the line tension.

As far as the comparison with experimental data is concerned one should keep in mind that the present analysis is based on a mean-field theory which neglects thermal fluctuations of the contact line along the  $z$  direction. Their contribution to the line tension as well as to the shape of the mean interface profile still awaits a thorough analysis. For a first step in that direction see Refs. [51, 74, 75]. Our present study serves as a prerequisite of such further analyses. The capillary-wavelike fluctuations of the liquid-vapor interface broaden the interfacial width of the density transition region around  $l(x)$ . For a free liquid-vapor interface these fluctuations lead to a roughening of the interface which is only limited by gravity or system size [76]. Model calculations for short-ranged forces show that this feature occurs also at the three-phase contact line [77]. Thus the shape  $l(x)$  of the interface will play a similar role as the intrinsic density profile of the liquid-vapor interface [76] as far as the roughening by capillary waves is concerned. It is not known yet whether these fluctuations can even induce a distortion of the loci of the liquid-vapor interface as compared to the function  $l(x)$  computed here.

## V. SUMMARY

Based on a microscopic density functional theory [Eq. (2.1)] we have obtained the following main results for the structural properties of the region of three-phase contact where the liquid-vapor interface of a liquid drop meets the supporting substrate at a contact angle  $\theta$ .

(1) By assuming a steplike density variation across the liquid-vapor interface the lateral shape  $l(x)$  of this interface minimizes the line contribution  $\tau[l(x)]$  of the corresponding grand canonical free energy. The minimum value is the line tension. Equations (4.1)–(4.8) provide the analytic expression for the explicit functional dependence of  $\tau[l(x)]$  on  $l(x)$ , on the underlying pair potential  $\phi(r)$  between the fluid particles, and on the substrate potential.

(2)  $\tau[l(x)]$  is a nonlocal functional of  $l(x)$  [Eq. (4.8)]. By enforcing a gradient expansion  $\tau[l(x)]$  can be cast into a local functional [Eq. (4.9)] which resembles the form commonly used in a phenomenological ansatz. This local theory must be regarded as an inferior approximation of the full nonlocal theory.

(3) The equilibrium profile  $l(x)$  has been determined numerically both for the local (Figs. 8 and 9) and the nonlocal theory (Figs. 10 and 11) as a function of temperature  $T$  and for different interaction potentials. For a system undergoing a first-order wetting transition  $l(x)$  approaches its asymptote on the liquid side from below (Figs. 8 and 10) whereas  $l(x)$  approaches this asymptote from above in the case of a continuous wetting transition (Figs. 9 and 11).

(4) Although both the local and the nonlocal theory predict qualitatively similar profiles there are large quantitative

differences between the local and nonlocal results for the absolute value and the lateral width of the deviation  $\delta l(x) = l(x) - a(x)$  of the profile from the asymptotes  $a(x)$  which are fixed by the surface free energies (see Figs. 10 and 11). Also the predictions for the curvature of  $l(x)$  differ significantly (Fig. 13). These differences increase upon approaching a wetting transition  $T_w$  at which the contact angle  $\theta$  vanishes (Fig. 12).

(5) There is no effective local theory which can reproduce the results of the nonlocal theory (Fig. 14). Thus for a quantitative analysis the local theory must be discarded.

(6) For first-order wetting the line tension is positive and diverges for  $T \rightarrow T_w$  [Fig. 16(a)] whereas for a continuous wetting transition it is negative and vanishes for  $T \rightarrow T_w$  [Fig. 16(a)] proportional to  $\theta^{1/3}$ . In the case of first-order wetting the line tension increases  $\sim 1/\theta$  although we cannot rule out a crossover to a behavior  $\sim \ln(1/\theta)$  very close to  $T_w$  as predicted by the local theory. Away from wetting transitions the absolute value of the line tension is of the order of  $\epsilon/\sigma$  where  $-\epsilon$  is the potential minimum of the pair potential  $\phi(r)$  and  $\sigma$  the diameter of the fluid particles. However, we emphasize that both  $l(x)$  and  $\tau$  do depend also on the substrate potential [see Eqs. (4.4) and (4.7)].

(7) A somewhat surprising result of the nonlocal theory is that the approximation of the actual smooth profile  $l(x)$  by its straight asymptotes  $a(x)$  is very good. Even in the core of the three-phase contact region the maximum absolute value of the deviation  $\delta l(x) = l(x) - a(x)$  is at most of the order of the diameter  $\sigma$  of the fluid particles [Figs. 10(a) and 11(a)]. However, the lateral width of this deviation, which may be regarded as the spatial extension of this three-phase contact region, reaches several hundred fluid diameters (see Fig. 12). Nonetheless the integrated deviation  $\int_{-\infty}^{\infty} dx \delta l(x)$  diverges upon approaching a wetting transition.

(8) Equations (4.4) and (4.6) provide a rather accurate, analytic estimate for the actual value of the line tension.

### ACKNOWLEDGMENTS

We gratefully acknowledge numerous helpful discussions with Professor M. Napiórkowski. We thank Dr. E. M. Blokhuis for providing us with unpublished results.

### APPENDIX: REFERENCE CONFIGURATIONS

The analysis in the main text is based on a systematic decomposition of the free energy given by Eq. (2.1) into bulk, surface, and line contributions. This requires one to study a finite size fluid sample with volume  $V$  which is truncated such that outside of  $V$  the fluid density is set to zero and called vacuum  $v$ . This truncation generates artificial surface and line contributions to the free energy which add to the one we are interested in due to three-phase coexistence around  $x = y = 0$ . Since the actual calculation yields only the sum of these physically relevant contributions and of the artificial ones we have to compute the artificial contributions separately by considering suitable reference configurations. Their knowledge enables us to subtract them from the aforementioned sum and to get access to the physically relevant contributions alone. One important artificial line contribution which appears in this calculation is the line contribution to

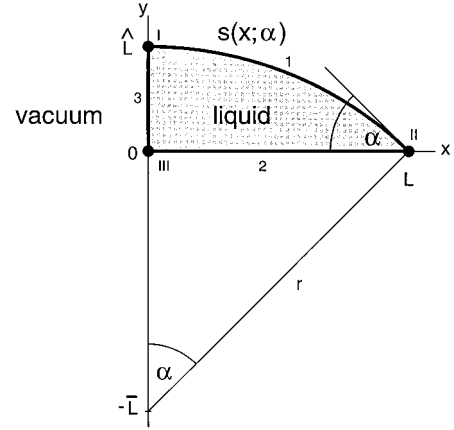


FIG. 17. Reference configuration for determining the line tension of a liquid wedge with arbitrary opening angle  $\alpha$  surrounded by vacuum. 1, 2, and 3 denote the surface tensions arising between the liquid and the surrounding vacuum. I, II, and III denote the line tensions arising from the edges of this liquid ridge which extends translationally invariantly into the  $z$  direction normal to the  $xy$  plane. In the thermodynamic limit the line tensions at I and III reduce to that of a rectangular liquid wedge surrounded by vacuum, denoted as  $\tau_{lvvv}$ , and the line tension II reduces to that of the corresponding liquid wedge with arbitrary opening angle  $\alpha$ , denoted as  $\tau_{lvvv}(\alpha)$ , so that  $\tau_{lvvv}(\alpha = \pi/2) = \tau_{lvvv}$ .  $L(\alpha) = r \sin \alpha$ ,  $\bar{L}(\alpha) = L(\alpha) \tan \alpha$ , and  $\hat{L}(\alpha) = r - \bar{L}(\alpha)$ . The arc of a circle is given by  $s(x; \alpha) = \sqrt{r^2 - x^2} - \bar{L}(\alpha)$  for  $0 \leq x \leq L$ .

the free energy generated by the edge of a wedgelike volume with an arbitrary opening angle  $\alpha$  filled homogeneously with a fluid and surrounded by vacuum. In order to solve this nontrivial problem it turned out that it is suitable to consider the reference configuration depicted in Fig. 17 which is translationally invariant in the  $z$  direction. The volume filled with liquid is part of a sector with radius  $r$  and opening angle  $\alpha$ . The liquid is surrounded by vacuum. The linear extensions of this system are characterized by  $L(\alpha) = r \sin \alpha$ ,  $\bar{L}(\alpha) = L(\alpha) \tan \alpha$ , and  $\hat{L}(\alpha) = r - \bar{L}(\alpha)$  (see Fig. 17). The arc, denoted as 1 in Fig. 17, is given by  $s(x; \alpha) = \sqrt{r^2 - x^2} - \bar{L}(\alpha)$  with  $0 \leq x \leq L$  and has the length  $s(\alpha) = \alpha r$ . The area of the cross section of the liquid filled segment perpendicular to the  $z$  axis is  $\tilde{A}^\perp(\alpha) = \frac{1}{2}[\alpha r^2 - L(\alpha)\bar{L}(\alpha)]$ . The linear extension in  $z$  direction is  $L_z$  for which we take periodic boundary conditions so that there are no additional surface and line contributions generated by truncating the liquid ridge at  $z = \pm L_z/2$ . The volume of this reference system is  $V(\alpha) = L_z \tilde{A}^\perp(\alpha)$ . Inserting the density distribution

$$\hat{\rho}(x, y; \alpha) = \rho_l \Theta(y) \Theta(s(x; \alpha) - y) \Theta(x) \Theta(L - x) \quad (\text{A1})$$

into Eq. (2.1) leads in the thermodynamic limit to the following bulk, surface, and line contributions:

$$\Omega(\alpha) = V(\alpha) \Omega_b(\rho_l, T, \mu) + \tilde{A}^\perp(\alpha) \Omega_s + L_z \Omega_l, \quad (\text{A2})$$

where  $\Omega_b$  is given by Eq. (2.9),  $\Omega_s = \sigma_{lv}$  where

$$\sigma_{lv} = -\frac{1}{2} \rho_l^2 \int_0^\infty dx t(x) \quad (\text{A3})$$

is the liquid-vacuum surface tension associated with the overall surface area  $\tilde{A}^{\parallel}$  of the liquid ridge:

$$\tilde{A}^{\parallel} = L_z [s(\alpha) + L(\alpha) + \hat{L}(\alpha)]. \quad (\text{A4})$$

In Fig. 17 the three liquid-vacuum surface tensions are denoted as 1, 2, and 3.

According to Fig. 17 there are three line contributions proportional to  $L_z$  due to the lines denoted as I, II, III in Fig. 17. In the thermodynamic limit  $L \rightarrow \infty$  the line contribution  $\Omega_l$  is the sum of these three individual line tensions. In this limit the line tensions due to I and III become equal to each other and are given by the line tension of a rectangular liquid wedge surrounded by vacuum:

$$\tau_{lvvv} = \frac{1}{2} \rho_l^2 \int_0^{\infty} dx \int_0^{\infty} dy \bar{t}(x, y), \quad (\text{A5})$$

where

$$\bar{t}(x, y) = \int_x^{\infty} dx' \int_y^{\infty} dy' \hat{w}(x'^2 + y'^2). \quad (\text{A6})$$

In the notation  $\tau_{abcd}$  the indices stand for the phases occupying the quadrants meeting at that line which the line tension  $\tau_{abcd}$  corresponds to;  $l$  stands for liquid and  $v$  for vacuum. Equations (A5) and (A6) are known independently from Ref. [60]. In the thermodynamic limit  $L \rightarrow \infty$  the line tension due to II reduces to that of a liquid wedge with an opening angle  $\alpha$  as discussed in the second paragraph of this appendix. This line tension is denoted by  $\tau_{lvvvv}(\alpha)$  which carries five indices because the first two form a pair since one quadrant is partly occupied by liquid and partly by vacuum (see Fig. 17). Thus we have  $\Omega_l(\alpha) = \tau_{lvvvv}(\alpha) + 2\tau_{lvvv}$  and find

$$\tau_{lvvvv}(\alpha) = \frac{1}{2} \rho_l^2 \left( 1 + \frac{\pi - \alpha}{\tan \alpha} \right) \int_0^{\infty} dx \int_0^{\infty} dy \bar{t}(x, y). \quad (\text{A7})$$

Equation (A7) is in accordance with a result obtained by Blokhuis [78], who considered the case of three phases meeting at angles  $\alpha$ ,  $\beta$ , and  $\gamma$ . Note that  $\tau_{lvvvv}(\alpha = \pi/2) = \tau_{lvvv}$  and  $\tau_{lvvvv}(\alpha = \pi) = 0$ .

With the knowledge of  $\tau_{lvvvv}(\alpha)$  we are in the position to determine all line contributions for the reference geometry considered in Fig. 18 which describes the case that the interface profile is approximated by its asymptotes  $a(x)$  [see Eq. (3.8)]:

$$\hat{\rho}(x, y) = \Theta(y - d_w) \{ \rho_l \Theta(a(x) - y) + \rho_g \Theta(y - a(x)) \} \Theta(L - |x|). \quad (\text{A8})$$

Inserting Eq. (A8) into Eq. (2.1) yields after a tedious calculation the following expression for the free energy of this configuration which depends on  $l_0$  and  $\theta$ :

$$\Omega(l_0, \alpha) = V^{(l)}(\theta) \Omega_b(\rho_l) + V^{(g)}(\theta) \Omega_b(\rho_g) + A^{\parallel} \Omega_s^{\parallel}(l_0, \theta) + A^{\perp}(\theta) \Omega_s^{\perp} + L_z \Omega_l(l_0, \theta). \quad (\text{A9})$$

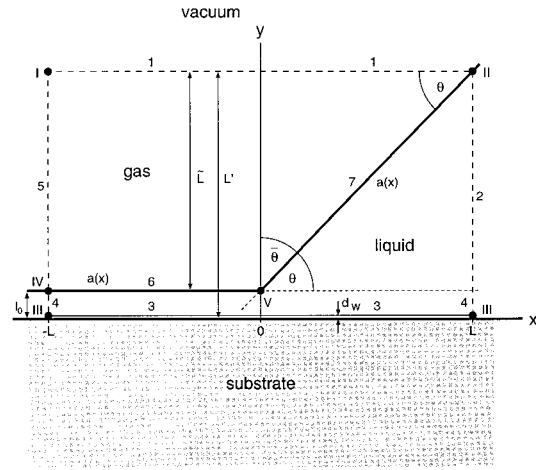


FIG. 18. Reference configuration for determining the bulk, surface, and line contributions to the free energy if the density configuration is given by the straight lines  $a(x)$  of the asymptotes [see Eq. (3.8)]. For  $x < 0$  the substrate is nonwet and covered by a microscopic film with thickness  $l_0$ . For  $x > 0$  the substrate is covered by liquid with a contact angle  $\theta$ . The system is truncated at  $x = \pm L$  and at  $y = L'$  and is surrounded by vacuum. The system is translationally invariant in the  $z$  direction normal to the  $xy$  plane. The Arabic numbers from 1 to 7 denote the corresponding surface tensions, whereas the Roman numbers I–V denote the corresponding line tensions.  $d_w$  indicates the excluded volume at the wall.

The bulk contributions are given by Eq. (2.9) and by  $V^{(l)}(\theta) = \frac{1}{2} LL_z \tilde{L}(\theta)$  and  $V^{(g)}(\theta) = \frac{3}{2} LL_z \tilde{L}(\theta)$  with  $\tilde{L}(\theta) = L \tan \theta$ . There are two types of surface contributions: a contribution which is proportional to the horizontal area  $A^{\parallel} = LL_z$  and one which is proportional to the vertical area  $A^{\perp}(\theta) = \tilde{L}(\theta) L_z$ . The surface contribution  $\Omega_s^{\parallel}(l_0, \theta)$  which corresponds to  $A^{\parallel}$  consists of the following terms:

$$\Omega_s^{\parallel}(l_0, \theta) = 2l_0 \Omega_b(\rho_l) + 2\sigma_{wl} + 2\sigma_{gv} + \sigma_{lg} + \frac{1}{\cos \theta} \sigma_{lg} + \omega(l_0). \quad (\text{A10})$$

The term  $2l_0 \Omega_b(\rho_l)$  stems from the liquid film of thickness  $l_0$ ;  $2\sigma_{wl}$  is the wall-liquid surface tension denoted as 3 in Fig. 18 which takes into account the excluded volume  $d_w$  [see Eq. (2.14) and Fig. 5]. The third term  $\sigma_{gv}$  stems from the truncation of the fluid sample at  $y = L'$ ; this gas-vacuum surface tension is indicated as 1 in Fig. 18 and its value is given by Eq. (A3) with  $\rho_l$  replaced by  $\rho_g$ . The fourth term in Eq. (A10) is the liquid-gas interface  $a(x < 0)$  denoted as 6 in Fig. 18. Similarly the liquid-gas interface  $a(x > 0)$  denoted as 7 in Fig. 18 gives rise to the term  $(1/\cos \theta) \sigma_{lg}$ . The last term  $\omega(l_0)$  in Eq. (A10) describes the interaction between wall-liquid interface (3) with the liquid-gas interface (6) at a distance  $l_0$  [see Eq. (2.19)]. The surface contribution  $\Omega_s^{\perp}$  is induced by the truncation of the fluid at  $x = \pm L$  and is the sum of the gas-vacuum and the liquid-vacuum surface tension:  $\Omega_s^{\perp} = \sigma_{gv} + \sigma_{lv}$  [see Eq. (A3)].

In Eq. (A9) the line contribution  $\Omega_l(l_0, \theta)$  collects all contributions to the free energy which scale with the system size  $L_z$  only. There are seven terms:

$$\begin{aligned} \Omega_l(l_0, \theta) = & 2(l_0 - d_w)\sigma_{lv} + \bar{\omega}(l_0, \theta) + \tau_{gvvv} + 2\tau_{lwww} \\ & + \delta\tau_{lgvv} + \tilde{\tau}_{lgvvv}(\theta) + \tilde{\tau}_{llgg}(\theta). \end{aligned} \quad (\text{A11})$$

The first term  $2(l_0 - d_w)\sigma_{lv}$  is due to the truncations at  $x = \pm L$  and is denoted as 4 in Fig. 18. The second term describes the interaction between the tilted gas-liquid interface and the substrate:

$$\begin{aligned} \bar{\omega}(l_0, \theta; L) = & \Delta\rho \left( \rho_l \int_0^L dx \int_{a(x)-d_w}^{\infty} dy t(y) \right. \\ & \left. - \rho_w \int_0^L dx \int_{a(x)}^{\infty} dy V(y) \right). \end{aligned} \quad (\text{A12})$$

For  $L$  fixed and  $\theta \rightarrow 0$  one has  $\bar{\omega}(l_0, \theta \rightarrow 0; L) = L\omega(l_0)$  with  $\omega(l_0)$  given by Eq. (2.19). In this limit  $\bar{\omega}(l_0, \theta = 0; L)$  would lead to a factor 2 in front of the last term in Eq. (A10) and thus to the correct effective interface potential for a flat wetting film because in Eq. (A10)  $\Omega_s^l(l_0, \theta)$  is measured in units of  $LL_z$  instead of  $2LL_z$  which is the total surface area of the substrate. This explains why in the thermodynamic limit

$$\bar{\omega}(l_0, \theta) := \bar{\omega}(l_0, \theta; L = \infty) \quad (\text{A13})$$

the contribution  $\bar{\omega}(l_0, \theta)$  diverges  $\sim 1/\theta$  for  $l_0$  fixed and  $\theta \rightarrow 0$  [see Eq. (4.4) which follows from Eqs. (A12) and (A13)]. Thus the thermodynamic limit  $L \rightarrow \infty$  and the limit  $\theta \rightarrow 0$  cannot be interchanged.  $\tau_{gvvv}$  and  $2\tau_{lwww}$  correspond to the dots indicated as I and III, respectively, in Fig. 18 which represent in an obvious notation the gas-vacuum-vacuum-vacuum line tension at  $(x, y) = (-L, L')$  and the liquid-wall-wall-vacuum line tension at  $(x, y) = (\pm L, 0)$ .  $\tau_{gvvv}$  is given by Eq. (A5) after replacing  $\rho_l$  by  $\rho_g$ . Since the liquid film is separated from the substrate by a vacuum layer of thickness  $d_w$  one has  $\tau_{lwww} = \tau_{lvvv}$ . The term

$$\delta\tau_{lgvv} = \tau_{lgvv} - \rho_l \Delta\rho \int_0^{\infty} dx \int_{l_0 - d_w}^{\infty} dy \bar{t}(x, y) \quad (\text{A14})$$

describes the line tension at  $(x, y) = (-L, l_0)$  denoted as IV in Fig. 18. This is the liquid-gas-vacuum-vacuum line tension

$$\tau_{lgvv} = \frac{1}{2}(\Delta\rho)^2 \int_0^{\infty} dx \int_0^{\infty} dy \bar{t}(x, y) \quad (\text{A15})$$

corrected by the fact that the quadrant filled with liquid is not infinitely thick but has only a finite thickness  $l_0$ . The expression

$$\begin{aligned} \tilde{\tau}_{lgvvv}(\theta) = & \frac{1}{2} \left[ \rho_g^2 \left( 1 + \frac{\pi - \theta}{\tan\theta} \right) - \rho_g \rho_l \left( 1 + \frac{\pi - \theta}{\tan\theta} + \frac{\pi - \bar{\theta}}{\tan\bar{\theta}} \right) \right. \\ & \left. + \rho_l^2 \left( 1 + \frac{\pi - \bar{\theta}}{\tan\bar{\theta}} \right) \right] \int_0^{\infty} dx \int_0^{\infty} dy \bar{t}(x, y), \end{aligned} \quad (\text{A16})$$

with  $\bar{\theta} = \pi/2 - \theta$  gives the line tension at  $(x, y) = (L, L')$  denoted as II in Fig. 18 which is generated by the meeting of the liquid and the gas phase under the angles  $\theta$  and  $\bar{\theta}$  and the vacuum. This provides also a self-explanatory notation as far as the five indices of  $\tilde{\tau}$  are concerned. The last term in Eq. (A11),

$$\tilde{\tau}_{llgg}(\theta) = \frac{1}{2} (\Delta\rho)^2 \left[ 1 + \frac{\theta}{\tan(\pi - \theta)} \right] \int_0^{\infty} dx \int_0^{\infty} dy \bar{t}(x, y), \quad (\text{A17})$$

represents the liquid-gas line tension at  $(x, y) = (0, l_0)$ , denoted as V in Fig. 18, in the limit  $l_0 \rightarrow \infty$ . The correction due to  $l_0 < \infty$  is contained in the term  $\bar{\omega}(l_0, \theta)$ . Note that as expected  $\tilde{\tau}_{llgg}(\theta \rightarrow 0) = 0$ . Equation (A17) can be transformed into Eq. (4.3) where we introduced the short notation  $\tilde{\tau}(\theta) = \tilde{\tau}_{llgg}(\theta)$ .

With these results the total line contribution can be grouped into physically relevant and into artificial contributions:

$$\Omega_l(l_0, \theta) = \Omega_l(l_0, \theta)_{\text{phys}} + \Omega_l(l_0, \theta)_{\text{art}}, \quad (\text{A18})$$

where

$$\Omega_l(l_0, \theta)_{\text{phys}} = \bar{\omega}(l_0, \theta) + \tilde{\tau}(\theta) \quad (\text{A19})$$

and  $\Omega_l(l_0, \theta)_{\text{art}} = \Omega_l(l_0, \theta) - \Omega_l(l_0, \theta)_{\text{phys}}$ . This leads to Eq. (4.2).

The explicit knowledge of the bulk, surface, and line contributions for the reference geometry shown in Fig. 18 enables us to determine the corresponding quantities for the actual case that the interface profile  $l(x)$  is not given by piecewise straight lines  $a(x)$  but by a smooth variation as in Figs. 8(a) and 9(a). Since  $l(|x| \rightarrow \infty) = a(x)$  the difference  $\delta l(x) = l(x) - a(x)$  vanishes for  $|x| \rightarrow \infty$ . This implies that both the bulk and the surface contributions of the free energy for the configuration  $l(x)$  are the same as for the case  $l(x) = a(x)$ . The line contribution corresponding to the configuration  $l(x)$  contains all terms present for  $l(x) = a(x)$  plus additional terms  $\tilde{\Omega}_l[l(x)]$  which vanish for  $l(x) = a(x)$ . Furthermore, all artificial free energy contributions are generated by the truncation of the sample at large distances. Since at these large distances the actual profile  $l(x)$  reduces to the asymptotes  $a(x)$ , the artificial contributions for the smooth case  $l(x)$  are identical to those for the case  $a(x)$  shown in Fig. 18. On the other hand, the difference  $\delta l(x)$  does not generate new artificial contributions. Therefore we can conclude that the physically relevant line contribution  $\Omega_l[l(x)]$  for the actual, smooth profile  $l(x)$  is the sum of  $\Omega_l(l_0, \theta)_{\text{phys}}$  [see Eq. (A19)] and  $\tilde{\Omega}_l[l(x)]$  (see above). A lengthy calculation shows that

$$\tilde{\Omega}_l[l(x)] = \tau_{\omega}[l(x)] + \tau_i^{(\text{nloc})}[l(x)], \quad (\text{A20})$$

where  $\tau_{\omega}[l(x)]$  is given by Eq. (4.7) and  $\tau_i^{(\text{nloc})}[l(x)]$  by Eq. (4.8).

- [1] J. W. Gibbs, *The Collected Works of J. Willard Gibbs* (Yale University Press, London, 1957), p. 288.
- [2] J. S. Rowlinson and B. Widom, *Molecular Theory of Capillarity* (Clarendon, Oxford, 1982).
- [3] P. G. de Gennes, *Rev. Mod. Phys.* **57**, 827 (1985).
- [4] S. Dietrich, in *Phase Transitions and Critical Phenomena*, edited by C. Domb and J. L. Lebowitz (Academic, London, 1988), Vol. 12, p. 1.
- [5] J. Gaydos and A. W. Neumann, *J. Colloid Interface Sci.* **120**, 76 (1987).
- [6] J. Drelich, J. D. Miller, and J. Hupka, *J. Colloid Interface Sci.* **155**, 379 (1993).
- [7] G. Navascués and P. Tarazona, *J. Chem. Phys.* **75**, 2441 (1981).
- [8] B. M. Law, *Phys. Rev. Lett.* **69**, 1781 (1992).
- [9] A. D. Alexandrov, B. V. Toshev, and A. Scheludko, *Colloids Surf.*, A **79**, 43 (1993).
- [10] B. M. Law, *Phys. Rev. Lett.* **72**, 1698 (1994).
- [11] E. B. Dussan, *Annu. Rev. Fluid Mech.* **11**, 371 (1979).
- [12] J. Drelich and J. D. Miller, *Colloids Surf.* **69**, 35 (1992).
- [13] J. Drelich, J. D. Miller, A. Kumar, and G. M. Whitesides, *Colloids Surf.*, A **93**, 1 (1994).
- [14] J. Drelich, *Pol. J. Chem.* (to be published).
- [15] I. B. Ivanov, P. A. Kralchevsky, and A. D. Nikolov, *J. Colloid Interface Sci.* **112**, 97 (1986).
- [16] D. Platikanov, M. Nedyalkov, and V. Nasteva, *J. Colloid Interface Sci.* **75**, 612 (1980).
- [17] D. Platikanov, M. Nedyalkov, A. Scheludko, and B. V. Toshev, *J. Colloid Interface Sci.* **121**, 100 (1988).
- [18] V. J. Novotny and A. Marmur, *J. Colloid Interface Sci.* **142**, 355 (1991).
- [19] I. B. Ivanov, P. A. Kralchevsky, A. S. Dimitrov, and A. D. Nikolov, *Adv. Colloid Interface Sci.* **39**, 77 (1992).
- [20] I. B. Ivanov, A. S. Dimitrov, A. D. Nikolov, N. D. Denkov, and P. A. Kralchevsky, *J. Colloid Interface Sci.* **151**, 446 (1992).
- [21] J. Drelich, *Colloids Surf.*, A **116**, 43 (1996).
- [22] M. V. Berry, *J. Phys. A* **7**, 231 (1974).
- [23] B. A. Pethica, *J. Colloid Interface Sci.* **62**, 569 (1977).
- [24] P. Tarazona and G. Navascués, *J. Chem. Phys.* **75**, 3114 (1981).
- [25] B. V. Toshev, D. Platikanov, and A. Scheludko, *Langmuir* **4**, 489 (1988).
- [26] C. Varea and A. Robledo, *Physica A* **183**, 12 (1992).
- [27] D. Beaglehole, *J. Phys. Chem.* **93**, 5900 (1989).
- [28] F. Brochard-Wyart, J.-M. di Meglio, D. Quéré, and P. G. de Gennes, *Langmuir* **7**, 335 (1991).
- [29] P. G. de Gennes, X. Hua, and P. Levison, *J. Fluid Mech.* **212**, 55 (1990).
- [30] D. Li, F. Y. H. Lin, and A. W. Neumann, *J. Colloid Interface Sci.* **142**, 224 (1991).
- [31] D. Li, *Colloids Surf.*, A **116**, 1 (1996).
- [32] M. E. R. Shannahan, *Adv. Colloid Interface Sci.* **39**, 35 (1992).
- [33] F. Brochard and P. G. de Gennes, *Langmuir* **7**, 3216 (1991).
- [34] B. V. Toshev and D. Platikanov, *Adv. Colloid Interface Sci.* **40**, 157 (1992).
- [35] B. V. Toshev and M. Z. Avramov, *Colloids Surf.*, A **75**, 33 (1993).
- [36] B. V. Toshev, *Colloid Polym. Sci.* **273**, 807 (1995).
- [37] B. V. Toshev and M. Z. Avramov, *Colloids Surf. A* **100**, 203 (1995).
- [38] B. Widom, *J. Phys. Chem.* **99**, 2803 (1995).
- [39] R. Bausch and R. Blossey, *Phys. Rev. E* **48**, 1131 (1993).
- [40] R. Blossey, *Int. J. Mod. Phys. B* **9**, 3489 (1995).
- [41] J. F. Joanny and P. G. de Gennes, *J. Colloid Interface Sci.* **111**, 94 (1986).
- [42] B. Widom and A. S. Clarke, *Physica A* **168**, 149 (1990).
- [43] B. Widom and H. Widom, *Physica A* **173**, 72 (1991).
- [44] C. Varea and A. Robledo, *Phys. Rev. A* **45**, 2645 (1992).
- [45] I. Szleifer and B. Widom, *Mol. Phys.* **75**, 925 (1992).
- [46] J. O. Indekeu, *Physica A* **183**, 439 (1992).
- [47] B. Widom, in *Condensed Matter Theories*, edited by L. Blum and F. B. Malik (Plenum, New York, 1993), Vol. 8, p. 589.
- [48] M. Schick and P. Taborek, *Phys. Rev. B* **46**, 7312 (1992).
- [49] C. Varea and A. Robledo, *Phys. Rev. E* **47**, 3772 (1993).
- [50] J. O. Indekeu, G. Backx, and G. Langie, *Physica A* **196**, 335 (1993).
- [51] J. O. Indekeu and A. Robledo, *Phys. Rev. E* **47**, 4607 (1993).
- [52] D. B. Abraham, F. Latrémolière, and P. J. Upton, *Phys. Rev. Lett.* **71**, 404 (1993).
- [53] H. T. Dobbs and J. O. Indekeu, *Physica A* **201**, 457 (1993).
- [54] E. M. Blokhuis, *Physica A* **202**, 402 (1994).
- [55] A. Robledo and J. O. Indekeu, *Europhys. Lett.* **25**, 17 (1994).
- [56] S. Perković, E. M. Blokhuis, and G. Han, *J. Chem. Phys.* **102**, 400 (1995).
- [57] J. O. Indekeu, *Int. J. Mod. Phys. B* **8**, 309 (1994).
- [58] R. E. Benner, L. E. Scriven, and H. T. Davis, *Faraday Symp. Chem. Soc.* **16**, 169 (1981).
- [59] M. Napiórkowski, W. Koch, and S. Dietrich, *Phys. Rev. A* **45**, 5760 (1992).
- [60] W. Koch, S. Dietrich, and M. Napiórkowski, *Phys. Rev. E* **51**, 3300 (1995).
- [61] R. Evans, in *Liquids at Interfaces*, Proceedings of the Les Houches Summer School Lectures, Session XLVIII, edited by J. Chavrolin, J. F. Joanny, and J. Zinn-Justin (Elsevier, Amsterdam, 1990), p. 1.
- [62] J. A. Barker and D. Henderson, *J. Chem. Phys.* **47**, 4714 (1967).
- [63] J. P. Hansen and I. R. McDonald, *Theory of Simple Liquids* (Academic, London, 1986).
- [64] N. F. Carnahan and K. E. Starling, *J. Chem. Phys.* **51**, 635 (1969).
- [65] D. E. Sullivan and M. M. Telo da Gama, in *Fluid Interfacial Phenomena*, edited by C. A. Croxton (Wiley, New York, 1986), p. 45.
- [66] M. Schick, in *Liquids at Interfaces*, Proceedings of the Les Houches Summer School Lectures, Session XLVIII, edited by J. Chavrolin, J. F. Joanny, and J. Zinn-Justin (Elsevier, Amsterdam, 1990), p. 415.
- [67] S. Dietrich and M. Napiórkowski, *Phys. Rev. A* **43**, 1861 (1991).
- [68] S. Dietrich, in *Phase Transitions in Surface Films 2*, Vol. 267 of *NATO Advanced Study Institute, Series B: Physics*, edited by H. Taub, G. Torzo, H. J. Lauter, and S. C. Fain (Plenum, New York, 1991), p. 391.
- [69] S. Dietrich and M. Napiórkowski, *Physica A* **177**, 437 (1991).
- [70] M. Napiórkowski and S. Dietrich, *Z. Phys. B* **89**, 263 (1992).
- [71] M. Napiórkowski and S. Dietrich, *Phys. Rev. E* **47**, 1836 (1993).
- [72] M. Napiórkowski and S. Dietrich, *Z. Phys. B* **97**, 511 (1995).
- [73] Equation (3.1) resembles more closely the Weeks-Chandler-

Andersen separation scheme (Ref. [63]) than the Barker-Henderson scheme used in Eq. (2.5). Nonetheless we adopt Eq. (3.1) for reasons of simplicity.

- [74] A. S. Clarke, J. Chem. Phys. **96**, 9073 (1992); **96**, 9078 (1992).
- [75] K. Sekimoto, R. Oguma, and K. Kawasaki, Ann. Phys. (N.Y.) **176**, 359 (1987).
- [76] D. Jasnow, Rep. Prog. Phys. **47**, 1059 (1984).
- [77] P. Upton (private communication).
- [78] E. Blokhuis (private communication).